# Physical properties of Be-Based fluoroperovskite compounds XBeF3 (X = K, Rb): a first-principles study

2 authors:

Md. Atikur Rahman
Pabna University of Science and Technology
**89** PUBLICATIONS   **533** CITATIONS

Sarah Chaba Mouna
Dr. Yahia Fares University of Médéa
**5** PUBLICATIONS   **4** CITATIONS

Physical properties of Be-Based fluoroperovskite compounds XBeF3 (X = K, Rb): a first-principles study

# Physical properties of Be-based fluoroperovskite compounds XBeF$_3$ (X = K, Rb): a first-principles study

**Sarah Chaba Mouna**[1,*] ⓘ **, Missoum Radjai**[1] ⓘ **, Md. Atikur Rahman**[2] ⓘ **, Abdelmadjid Bouhemadou**[3] ⓘ **, Abdullah**[4]**, Djamel Houatis**[1]**, Djamel Allali**[5,6]**, Saber Sâad Essaoud**[7] **and Hatem Allaf**[1]

[1] Laboratory of Physics of Experimental Techniques and Their Applications (LPTEAM), University of Medea, Medea, Algeria
[2] Departments of Physics, Pabna University of Science and Technology, Pabna 6600, Bangladesh
[3] Laboratory for Developing New Materials and their Characterizations, Department of Physics, Faculty of Sciences, Ferhat Abbas University—Setif 1, 19000 Setif, Algeria
[4] Department of Physics, Kohat University of Science and Technology Kohat, Kohat 26000, Pakistan
[5] Physics and Chemistry of Materials Lab, Department of Physics, University of M'sila, 28000 M'sila, Algeria
[6] University of M'sila, Faculty of Technology, B.P. 166 Ichbilia, 28000 M'sila, Algeria
[7] Faculté des sciences, Département de physique, Laboratoire de Physique des Particules et Physique Statistique, Ecole Normale Supérieure-Kouba, BP 92, Vieux-Kouba 16050, Algérie

E-mail: sarahchahbamouna@gmail.com

CrossMark

## Abstract

In this study, we used the *ab-initio* computational tools as implemented in the CASTEP code to explore the effects of pressure on the structural, elastic, electronic, thermodynamic and optical properties of the fluoroperovskite compounds XBeF$_3$ (X = K, Rb) based on Being. Exchange–correlation interactions were modeled using the GGA-PBEsol functional. The ground state of the title materials was characterized by calculating the optimized lattice parameter, the bulk modulus $B$ and its pressure derivative, and the Goldsmith tolerance factor. These materials exhibit structural stability in the cubic structure even when subjected to significant pressure levels, extending up to 18 GPa. The analysis of numerical assessments of single-crystal elastic constants ($C_{ij}$), polycrystalline elastic moduli, namely shear modulus ($G$), Young's modulus and Poisson's ratio, as well as the anisotropy factor ($A$), highlights the mechanical stability, elastic anisotropy and ductility of considered the compounds. The thermodynamic properties of these materials were studied through the Debye quasi-harmonic model. Analysis of energy band structures and density of states spectra shows that XBeF$_3$ (X = K, Rb) is insulating in nature, with band gaps of 7.99 and 7.26 eV, respectively. Additionally, we calculated the linear optical spectra, including dielectric function, absorption coefficient, refractive index, optical reflectivity, and energy loss function. Based on the results obtained, these materials could be used in various optoelectronic devices operating in the UV spectrum and in energy storage devices.

---

* Author to whom any correspondence should be addressed.

## 1. Introduction

Scientists of materials have continually developed perovskite compounds with improved properties in recent years. Perovskites have the well-known formula as $ABX_3$; in which A can be a large cation, B can be a small cation, and oxygen/halide can be placed at X position. If X is occupied by fluorine, then the resultant structure formed is called as fluoroperovskite [1]. Fluoride perovskites ($ABF_3$), which are known for their geometrical and physical characteristics such as photoluminescence [2], piezoelectricity [3], ferroelectricity [4], semiconducting [5], antiferromagnetism [6] and optical properties [7–9], are very attractive. These compounds have been applied in various fields, such as in optics, medical science, magnets, lenses, semiconductors and sometimes as energy storage devices [10–13].

Technological requirements of semiconductor lithography require finer details, which require shorter wavelength lithography light [14]. As such, vacuum-ultraviolet-transparent materials are ideal for lenses in optical lithography steppers. Perovskite fluorides are good candidates for this purpose because of their large band gaps. The cubic perovskite structure is more suitable as a lens material because it has no birefringence which complicates lens design [10]. Utilizing the technique of Czochralski, Shimamura, and Fukuda successfully cultivated single crystals of $KMgF_3$ and $BaLiF_3$, subsequently conducting precise measurements of their absorption edges at a wavelength of 115 nm ([15] 10.8 eV) and 123 nm [16] (10.1 eV). Nishimatsu and co-workers [10] carried out an investigation of perovskites with the objective of employing them as lens materials in optical lithography steppers. Following that, research was conducted on the fabrication of light emitting diode in vacuum ultraviolet range through the use of a solid solution $LiBaCaSrF_3$ on $LiSrF_3$ [17] as well as $LiKBaMgF_3$ on $LiBaF_3$ for deep-ultraviolet [18]. These applications require materials with direct band gaps. $ACaF_3$ (A = K, Rb, Cs) have been investigated as potential active materials for core-valence luminescence [19]. Cui *et al* [20] conducted a first-principles study of the effect of pressure on the structural, electronic and optical properties of $KMgF_3$. It was found that $KMgF_3$ is an insulator of a wide indirect band gap even under pressure effect up to 100 GPa. In addition to K-based fluoro-perovskites, Ag-based fluoro-perovskite materials have been studied in recent years [21–23]. Larbi *et al* [24] used the FP-LAPW technique to explore the conduct of the electrical and structural characteristics of $RbZnF_3$ under the stress up to 10 GPa. They observed that it has an indirect band gap. Creating new halide-based perovskites is fascinating because they reveal a wide range of incredible properties, they are technologically applicable and can include virtually every element in the periodic table [25]. Rai *et al* employed the modified Becke–Johnson exchange potential to examine the physical properties of $RbMF_3$ compounds (M = Be, Mg,

Ca, Sr, and Ba). The study revealed that $RbBeF_3$ has a large band gap [26] of 6.71 eV. A theoretical study for 10 perovskite crystals with the composition $IAIIAF_3$ (IA = K, Rb; IIA = Be, Mg, Ca, Sr, Ba) was carried out using the CRYSTAL09 software by Li *et al* [27]. They showed how these properties vary in relation to the alkaline-earth metal ions' Ionic radius *R* [27]. Khan *et al* [28] examined the structural electronic and optical properties of $TiXF_3$ (X = Ca, Cd, Hg, Mg) using GGA + U approximation and found that they have an isolating nature and could be used in scintillation detectors. Gómez-Peralta and Bokhimi [29] employed an Artificial Neural Network to predict 134 compounds of $AMX_3$ (where X represents F, Cl, Br, or I, and M denotes an alkali or earth-alkali element) that have a potential to adopt a cubic perovskite structure. The study revealed that these projected perovskites hold promising prospects for applications, including novel solar cells or transparent semiconductors [29]. Among the above-mentioned phases, we concentrated on $XBeF_3$ (X = K, Rb) fluoroperovskites with the aim of understanding the influence of pressure up to 18 GPa on their fundamental physical properties by employing the DFT versatile simulation implemented in the CASTEP code. Though some theoretical works are available in literature on these compounds, the study of the effect of high pressure on the physical features of $XBeF_3$ (X = K, Rb) is still missing. Therefore, we have studied the pressure effects on the structural, mechanical, thermodynamic, electronic, and optical properties of $RbBeF_3$ and $KBeF_3$ compounds by employing a pseudopotential plane-wave (PP-PW) method based on density functional theory (DFT) with the generalized gradient approximation (GGA) embodied in the CASTEP code.

The organizational framework of this paper is structured as follows: section 2 explains the computational methodologies. Section 3 is dedicated to the presentation and in-depth discussion of the results of the study. The section 4 succinctly describes the main conclusions and contributions derived from our research efforts.

## 2. Computational methods

The physical properties of $XBeF_3$ (X = K, Rb) compounds were studied using the pseudopotential plane wave (PP-PW) approach within the framework of DFT a [32] s implemented in the CASTEP code [31]. The PBEsol version of the GGA (GGA-PBEsol) [30] was used to model exchange–correlation interactions. Ultra-soft OTFG pseudopotentials were employed to address the interactions between core ions and valence states (K: $3s^2 3p^6 4s^1$; Rb: $4s^2 4p^6 5s^1$; Be: $1s^2 2s^2$, and F: $2s^2 2p^5$). The electron wave functions were developed into a plane wave basis set delimited by a cutoff energy of 650 eV. Brillouin zone (BZ) integrations were replaced by a summation on a $12 \times 12 \times 12$ Monkhorst Pack *k*-point grid [33]. The Broyden–Fletcher–Goldfarb–Shanno minimization

technique was employed to attain the equilibrium state of the structural parameters [34]. In order to obtain the geometry optimization, the convergence criteria were set as follows: $5.0 \times 10^{-6}$ eV/atom for the total energy, 0.01 eV Å$^{-1}$ for the maximal force, 0.02 GPa for the maximal stress, and $5.0 \times 10^{-4}$ Å for le maximum displacement. The elastic stiffness constants ($C_{ij}$) were calculated employing the stress–strain routine [35, 36]. The thermodynamic characteristics were computed using the quasi-harmonic approximation as incorporated in the Gibbs software [37]. The electronic and optical properties were calculated for the optimized geometry of XBeF$_3$ (X = K, Rb) by setting the $k$-point separation to 0.086 Å$^{-1}$, which corresponds to a $k$-point grid of $24 \times 24 \times 24$.

## 3. Results and discussion

### 3.1. Structural properties

The studied ternary Be-based fluoroperovskite materials XBeF$_3$ (X = K, Rb) crystallize in a CaTiO$_3$-type structure, i.e., cubic perovskite, with the Pm$\bar{3}$m space group (No. 221) and one formula unit in the unit cell ($Z = 1$) [29]. The X, Be, and F atoms occupy the following Wyckoff sites 1$a$ (0, 0, 0), 1$b$ (1/2, 1/2, 1/2) and 3$c$ (1/2, 1/2, 0), respectively. Figure 1. Shows a unit cell of the cubic perovskite KBeF$_3$ as a prototype of the cubic perovskite. The calculated equilibrium lattice constant ($a_0$) at zero temperature and zero pressure is 3.676 Å for KBeF$_3$ and 3.795 Å for RbBeF$_3$. The calculated equilibrium lattice parameters for both KBeF$_3$ and RbBeF$_3$ are in excellent agreement with the available counterparts in the literature [19, 26, 29], where the discrepancies are less than 0.073% and 0.2%, respectively, as shown in table 1.

It is noted that the lattice parameter of RbBeF$_3$ is larger than that of KBeF$_3$, which is attributed to the increasing size of the rubidium atom, which is the largest. To evaluate the coefficient of compressibility ($B$) and its pressure derivative ($B'$), we computed a series of total energy ($E$) versus unit cell volume ($V$) and the obtained $E(V)$ data were fitted to Birch's equation of state [38], as shown in figure 2. Moreover, the pressure versus unit cell volume data were fitted to the Birch–Murnaghan and Vinet equations [39, 40] as shown in figure 3. From table 1, it can be seen that the calculated values of the bulk modulus ($B$) from different fits with different equations of state (EOS) are practically equal, highlighting the reliability of the results obtained. Note that the $B$ value of RbBeF$_3$ is somewhat lower than that of KBeF$_3$, indicating that RbBeF$_3$ is more compressible than KBeF$_3$.

To evaluate the structural stability of the considered compounds, the Goldsmith tolerance factor ($t$) was calculated via the following relationship [41]:

$$t = \frac{r_A + r_X}{\sqrt{2}\,(r_B + r_X)}.$$

In this context, the symbols $r_A$, $r_B$, and $r_X$ represent the respective ionic radii of the A, B, and X ions within the composition of ABX$_3$ compounds. In cases where the computed
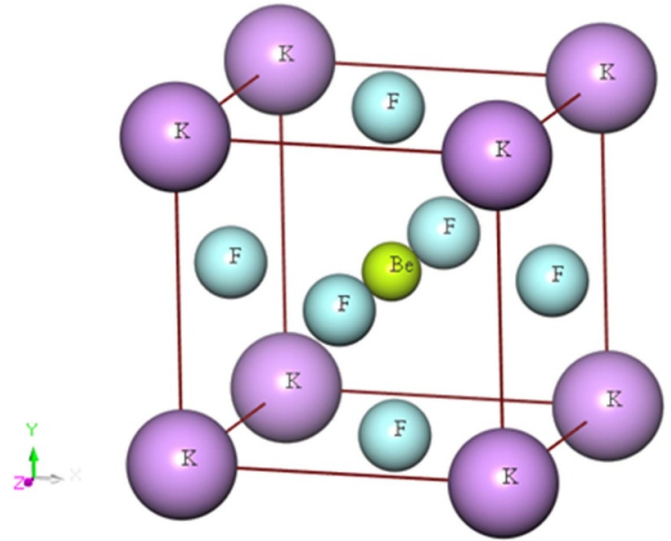


**Figure 1.** Crystal structure of KBeF$_3$ cubic perovskite.

value of '$t$' falls within the range of 0.81–1.10, it is deemed indicative of the stability of the perovskite structure [42]. The calculated '$t$' value is 1.25 for KBeF$_3$, and 1.29 for RbBeF$_3$, confirming that, the crystal structure stability of these compounds cannot be predicted by the Goldsmith tolerance factor. Therefore, we also calculated the formation enthalpy $\Delta H$ to check their thermodynamic stability using the following expression [43]:

$$\Delta H = \frac{1}{n_X + n_{Be} + n_F} \times \left[ E_{tot}^{XBeF_3} - \left( n_X E_{tot}^{X(solid)} + n_{Be} E_{tot}^{Be(solid)} + n_F E_{tot}^{F(solid)} \right) \right].$$

In this context, $E_{tot}^{XBeF_3}$ is the total energy of XBeF$_3$ (X = K, Rb), and $E_{tot}^{X(solid)}$, $E_{tot}^{Be(solid)}$ and $E_{tot}^{F(solid)}$ represent the total energy per atom in the solid state of the individual elements X, Be, and F, respectively, $n_X$, $n_{Be}$ and $n_F$ indicate the total number of X, Be and F atoms that the unit cell hold. Table 1 displays the computed results of the formation enthalpy, which are negative. This observation serves as an indicator of the thermodynamic stability exhibited by ternary XBeF$_3$ compounds, with X representing either K or Rb.

We performed calculations to study the effect of pressure on the unit cell volume ($V$) and the lattice parameter ($a$) of XBeF$_3$ materials by calculating '$a$' and '$V$' under different pressures in the range of 0 GPa to 18 GPa. Variations of $a/a_0$ and $V/V_0$ ($a_0$ and $V_0$ are the lattice parameter and unit cell volume at zero pressure, respectively) versus pressure are shown in figure 4. It is evident that $a/a_0$ and $V/V_0$ decrease with increasing pressure, which is explained by the decrease in atom distances with increasing pressure [44]. The variation of $a/a_0$ and $V/V_0$ with pressure is well proportional to third-order polynomials:

$$KBeF_3 \begin{cases} \dfrac{a}{a_0} = 1 - 3.33 \times 10^{-3} p + 8.77 \times 10^{-5} P^2 - 1.96 \times 10^{-6} p^3 \\[2mm] \dfrac{V}{V_0} = 1 - 1 \times 10^{-2} p + 3.04 \times 10^{-4} P^2 - 7.11 \times 10^{-6} p^3 \end{cases}$$

**Table 1.** Computed equilibrium lattice parameter (*a*, in Å unit), bulk modulus (*B*, in GPa) and its pressure derivative (*B'*), tolerance factor (*t*), ionic radii (*R*, in Å unit), formation enthalpy (Δ*H* in eV/atom unit) and bond length (d, in Å unit) for the $XBeF_3$ (X = K, Rb) materials compared with the available theoretical data.

| Parameters | KBeF$_3$ | | | RbBeF$_3$ | |
| --- | --- | --- | --- | --- | --- |
| | This work | | Other | This work | Other |
| *a* | 3.676 79 | | 3.6795 [d] | 3.795 38 | 3.8030 [d] |
| | | | | | 3.8431 [e] |
| | | | | | 3.8457 [f] |
| *B* | 102.99[a],102.29[b], 102.71[c] | | | 97.95[a], 97.48[b], 97.94[c] | 86.021[b] |
| *B'* | 4.412[a],4.409[b], 4.414[c] | | | 4.546[a], 4.511[b], 4.514[c] | 4.879[b] |
| Ionic radii (*R*) | *R*(K) | 1.51 | | | |
| | *R*(Rb) | 1.61 | | | |
| | *R*(Be) | 0.27 | | | |
| | *R*(F) | 1.33 | | | |
| *t* | 1.25 | | | 1.29 | |
| Δ*H* | −3.53 | | | −3.39 | |
| Bond length (*d*) | *d*(F–K) | 2.59 | | *d*(F–Rb) | 2.68 |
| | *d*(F–Be) | 1.83 | | *d*(F–Be) | 1.89 |
| | *d*(F–F) | 2.59 | | *d*(F–F) | 2.68 |

[a] From Birch *E–V* EOS [38].
[b] from Birch–Murnaghan *P−V* EOS [39].
[c] from Vinet *P−V* EOS [40].
[d] Gómez-Peralta and Bokhimi [29].
[e] Rai *et al* [26].
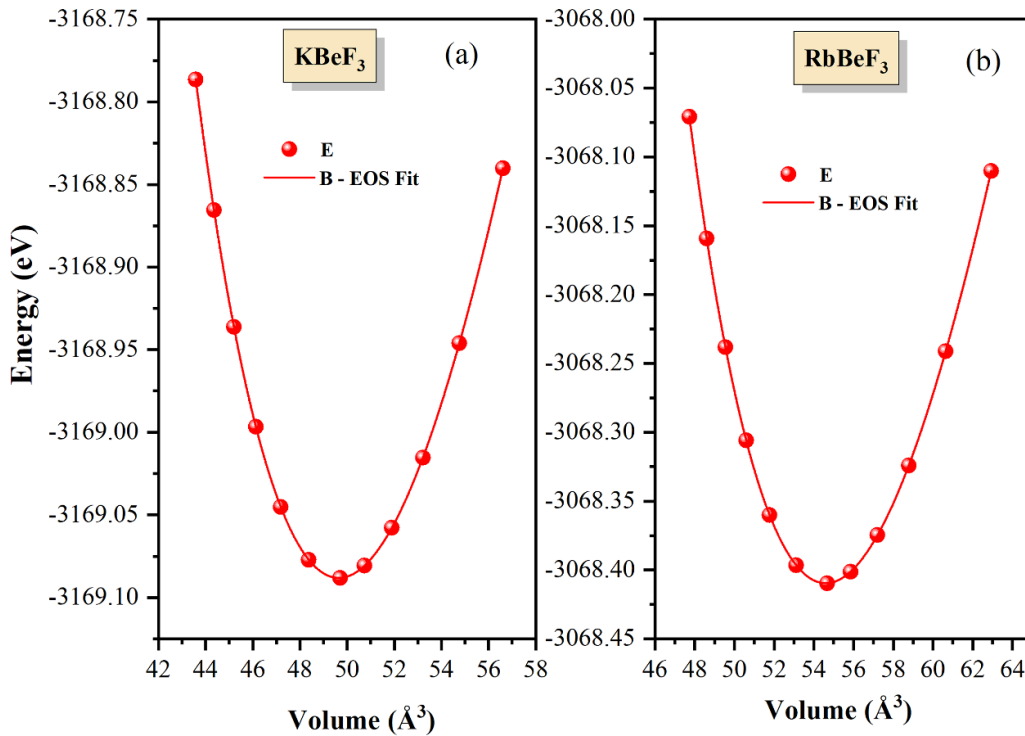[f] Syrotyuk and Shved [19].



**Figure 2.** Total energy versus unit cell volume (*E–V*) for (a) KBeF$_3$ and (b) RbBeF$_3$. The symbols indicate computed findings, whereas the continuous lines are the fits to the Birch's equations of state.

$$RbBeF_3 \begin{cases} \frac{a}{a_0} = 1 - 3.51 \times 10^{-3}p + 1.025 \times 10^{-4}P^2 - 2.44 \times 10^{-6}p^3 \\ \frac{V}{V_0} = 1 - 1.05 \times 10^{-2}p + 3.55 \times 10^{-4}P^2 - 8.79 \times 10^{-6}p^3 \end{cases}.$$

The calculated linear and volume compressibilities ($\beta_a$ and $\beta_V$) are $3.33 \times 10^{-3}$ and $1 \times 10^{-2}$, respectively, for KBeF$_3$,

and $3.51 \times 10^{-3}$ and $1.05 \times 10^{-2}$, respectively, for RbBeF$_3$. The bulk modulus *B* can be deduced from the linear and volume compressibilities as follows [45]: By applying the previously mentioned relationships, the calculated *B* values for KBeF$_3$ and RbBeF$_3$ are estimated to be approximately 100 GPa and 95 GPa, respectively. It is noteworthy that these
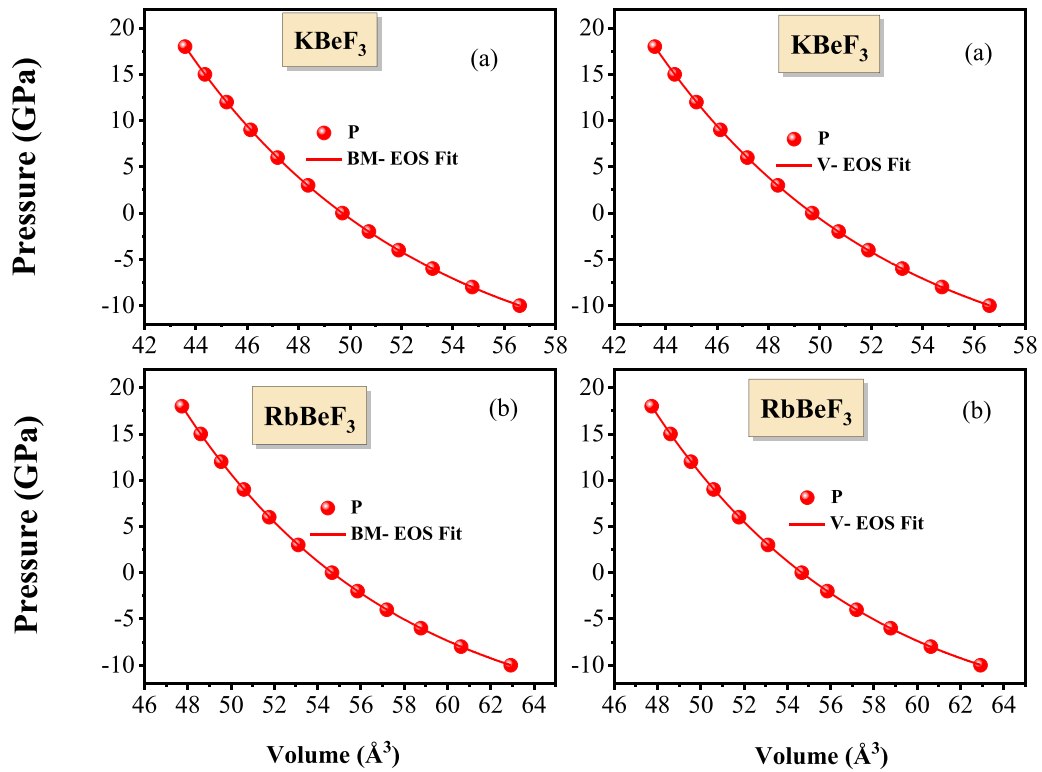
**Figure 3.** The computation of total energy versus pressure (*P–V*) for (a) KBeF$_3$ and (b) RbBeF$_3$. The symbols indicate computed findings, whereas the continuous lines are the fits to the Birch–Murnaghan and the Vinet equations of state (EOS).
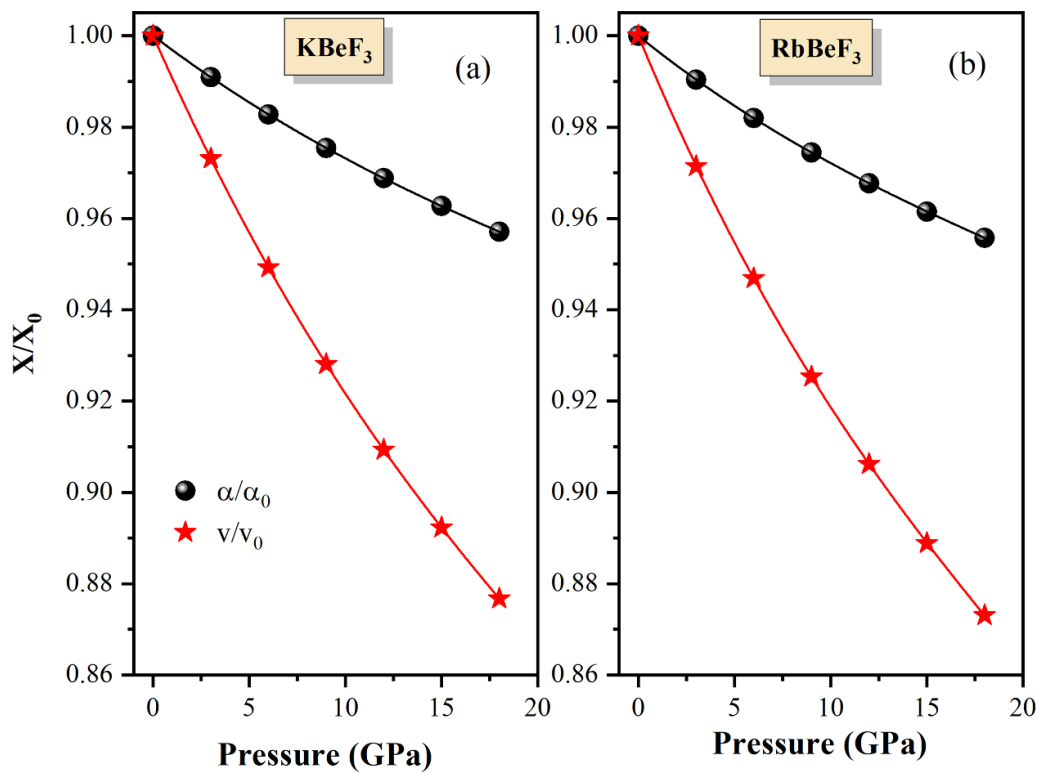


**Figure 4.** Variations of *a*/*a*$_0$ and *V*/*V*$_0$ with the pressure for (a) KBeF$_3$ and (b) RbBeF$_3$.

**Table 2.** Calculated monocrystalline elastic constants ($C_{ij}$, in GPa unit) for XBeF$_3$ (X = K, Rb) compounds, compared to results available in the literature.

| Compounds | | $C_{11}$ | $C_{12}$ | $C_{44}$ |
|---|---|---|---|---|
| KBeF$_3$ | Present work | 128.8 | 89.9 | 98.3 |
| RbBeF$_3$ | Present work | 114.4 | 89.7 | 95.1 |
| | Other [27] | 145.2 | 94.8 | 111.0 |
| | Other [27] | 131.1 | 94.0 | 109.5 |

values closely align with the corresponding results derived from the fitting of the *E–V* and *P–V* data to the appropriate EOS, as presented in table 1. This consistency serves as compelling evidence supporting the reliability and accuracy of the obtained outcomes.

## 3.2. Elastic properties

### 3.2.1. Monocrystalline elastic constants.
The monocrystalline elastic constants have an important part in offering significant information into the stability of stiffness and bonding characteristics of the material. Calculation of elastic constants is an essential technique for evaluating the mechanical stability of crystal, elastic anisotropy, stiffness, ductility, Debye temperature, and propagation of elastic waves inside materials. To provide an accurate depiction of elastic properties of a cubic crystal, 3 independent monocrystalline elastic constants, namely $C_{11}$, $C_{12}$, and $C_{44}$, are required [46]. The numerical estimates of the elastic constants of KBeF$_3$ and RbBeF$_3$ at zero pressure are given in table 2 along with reported results from previous calculations [27]. The computed values of $C_{ij}$ for the XBeF$_3$ compounds, with X representing either K or Rb, demonstrate a level of agreement that is deemed acceptable when compared to the findings of previous theoretical investigations documented in the existing literature [27]. To be mechanically stable, the elastic constants of a cubic system should satisfy the mechanical stability criteria [47, 48]: ($C_{11} - C_{12}$) > 0; ($C_{11} + 2C_{12}$) > 0; $C_{11}$ > 0; $C_{44}$ > 0; $C_{12}$<$B$ < $C_{11}$. All of the conditions outlined previously are met by the computed values of the elastic constants for the materials under consideration, affirming their mechanical stability. The computed value of C$_{11}$, which characterizes the material's resistance to compressional strain along the [100] crystallographic direction, surpasses that of $C_{44}$, which signifies the material's resistance to shear deformation within the (100) plane along the same primary direction [100]. This outcome underscores that the materials exhibit a greater capacity to withstand unidirectional compression compared to shear deformation.

Figure 5 shows the pressure dependence of $C_{ij}$ of XBeF$_3$ (X = K, Rb) in a pressure range of 0–18 GPa. The calculated $C_{ij}(P)$ satisfy the mechanical stability conditions under pressure [49]: $C_{11} - P > |C_{12} + P|$; $C_{11} - P > 0$; $C_{44} - P > 0$; $C_{11} + 2C_{12} + P > 0$, highlighting the mechanical stability of the title compounds even under pressure effect up to 18 GPa. All $C_{ij}$s increase with increasing pressure, and their variations with pressure are well fitted to the following second-order polynomials:

$$\text{KBeF}_3 \begin{cases} C_{11} = 129.12 + 5.78P + 1.7 \times 10^{-2}P^2 \\ C_{12} = 90.34 + 2.58P + 2.23 \times 10^{-2}P^2 \\ C_{44} = 98.34 + 2.18P - 7.62 \times 10^{-3}P^2 \end{cases}$$

$$\text{RbBeF}_3 \begin{cases} C_{11} = 114.28 + 5.78P - 4.41 \times 10^{-3}P^2 \\ C_{12} = 89.58 + 3.34P + 6.79 \times 10^{-4}P^2 \\ C_{44} = 95.20 + 2.34P - 9.45 \times 10^{-3}P^2 \end{cases}.$$

### 3.2.2. Polycrystalline elastic parameters.
The single-crystal elastic constants can be used to estimate the isotropic elastic moduli, such as coefficient of compressibility *B* and shear modulus *G*, which are utilized to describe the elastic properties of multi-crystal aggregate and may be readily determined using the Voigt–Reuss–Hill (VRH) approximations [50, 51]. In the framework of the VRH approximations, the elastic moduli for the cubic XBeF$_3$ (X = K, Rb), namely bulk modulus (*B*), shear modulus (*G*), Young's modulus (*E*) and Poisson's ratio (σ), are computed using the following relationships [52–54]:

$$B = \frac{1}{3}\left(C_{11} + 2C_{12}\right)$$

$$G = \frac{1}{2}\left(\frac{C_{11} - C_{12} + 3C_{44}}{5} + \frac{5C_{44}\left(C_{11} - C_{11}\right)}{4C_{44} + 3\left(C_{11} - C_{12}\right)}\right)$$

$$E = \frac{9BG}{3B + G}$$

$$\sigma = \frac{3B - E}{6B}.$$

The calculated values of the aforementioned elastic moduli for the considered compounds are listed in table 3. The pressure-induced variations on *B*, *G*, and *E* are depicted in figure 5, which can be accurately described by second-order polynomials:

$$\text{KBeF}_3 \begin{cases} B = 103.27 + 3.83P + 2.05 \times 10^{-2}P^2 \\ E = 133.83 + 5.34P - 1.68 \times 10^{-2}P^2 \\ G = 52.11 + 2.1P - 9.27 \times 10^{-3}P^2 \end{cases}$$

$$\text{RbBeF}_3 \begin{cases} B = 97.81 + 4.18P - 1.02 \times 10^{-3}P^2 \\ E = 43.98 + 2.07P - 1.02 \times 10^{-2}P^2 \\ G = 114.47 + 5.34P - 2.34 \times 10^{-2}P^2 \end{cases}.$$

Based on the results obtained from the above calculations, we are able to make the following conclusions:

● The computed values of the bulk modulus from the $C_{ij}$ values are in good accord with the corresponding values obtained from the fits of *E–V* and *P–V* to the corresponding EOS, demonstrating the accuracy and dependability of the present calculations.
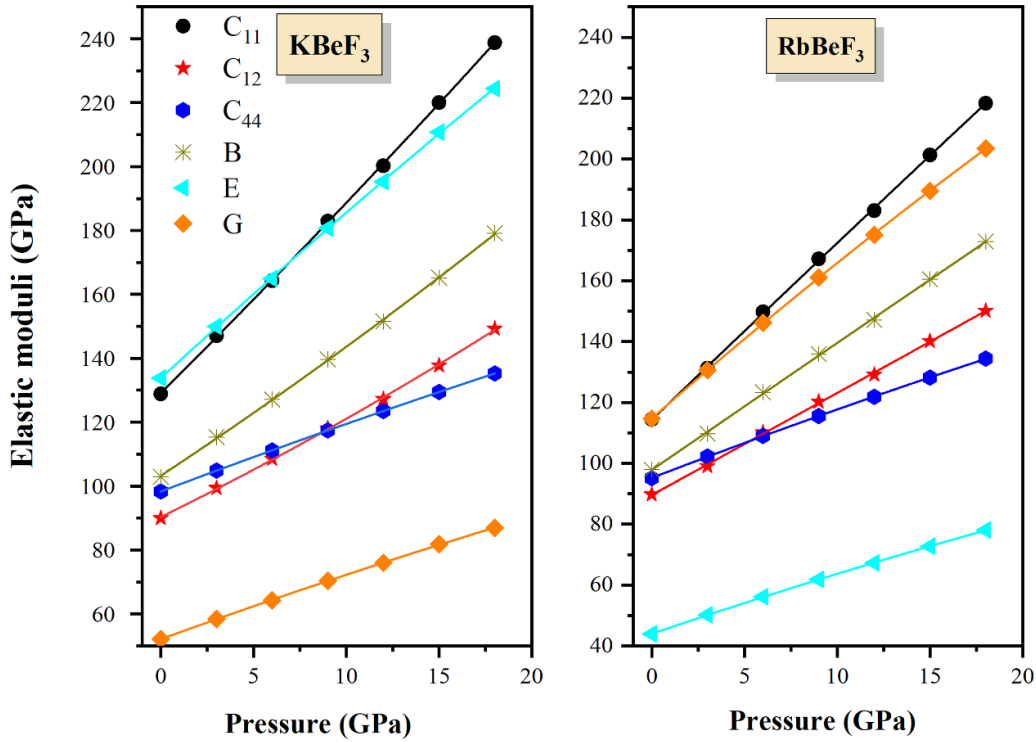
**Figure 5.** Developments of the elastic moduli $C_{11}$, $C_{12}$, $C_{44}$, *B*, *G* and *E* with pressure for (a) KBeF$_3$ and (b) RbBeF$_3$ compounds.

**Table 3.** Calculated bulk modulus (*B*, in GPa unit); shear modulus (*G*, in GPa unit); Young's modulus (*E*, in GPa unit); Poisson's ratio ($\sigma$, dimensionless), transverse, longitudinal, and average sound wave velocities ($V_t$, $V_l$, and $V_m$, in m s$^{-1}$ unit) and Debye temperature ($\theta_D$, in K unit) for KBeF$_3$ and RbBeF$_3$ compounds.

| Compound | *B* | *G* | *B/G* | *E* | $\sigma$ | $V_l$ | $V_t$ | $V_m$ | $\theta_D$ |
|---|---|---|---|---|---|---|---|---|---|
| KBeF$_3$ | 102.9 | 52.1 | 1.9 | 133.7 | 0.28 | 7007.9 | 3852.7 | 4294.5 | 594.5 |
| RbBeF$_3$ | 97.9 | 43.9 | 2.2 | 114.6 | 0.30 | 5833.2 | 3089.6 | 3453.2 | 463.0 |

- Pugh [55] established an empirical criterion to differentiate the brittleness and ductility of materials. According to this criterion, a material having *B/G* ratio greater than 1.75 is classified as of ductile nature, whereas brittleness nature will appear for a *B/G* ratio lower than 1.75. In the pressure range of 0–18 GPa, both compounds, XBeF$_3$ (X = K, Rb) have *B/G* ratios higher than 1.75, confirming their ductile nature across all pressure ranges. We can see from table 3 that RbBeF$_3$ is more ductile than KBeF$_3$, which is mostly due to the difference in ionic radii (*R*) between K and Rb atoms, notably, Rb has an upper *R*-value than K.
- Figure 5 demonstrates that KBeF$_3$ has a larger Young's modulus than RbBeF$_3$, indicating that KBeF$_3$ is substantially stiffer than RbBeF$_3$.
- Higher values of Poisson's ratio ($\sigma > 0.26$) indicate the ductility of the material, while lower values ($\sigma < 0.26$) indicate its brittleness [56]. Estimated Poisson's ratio values suggest that the title compounds are ductile in nature. This conclusion supports the findings obtained from Pugh's ratio.
- Debye temperature $\theta_D$ is an essential parameter that is directly related to several thermodynamic characteristics, such as specific heat, melting temperature, coefficient of thermal expansion and heat conductivity. The Debye temperature

can be computed using the well-known common relationship, which is related to the value of the average velocity of the elastic waves ($V_m$) [47, 57]:

$$\theta_D = \frac{h}{k_B} \left[ \left( \frac{3n}{4\pi} \right) \frac{N_A \rho}{M} \right]^{1/3} \times v_m \text{ where}$$

$$v_m = \left[ \frac{1}{3} \left( \frac{2}{v_t^3} + \frac{1}{v_l^3} \right) \right]^{-1/3}, \quad v_l = \left( \frac{3B + 4G}{3\rho} \right)^{1/2} \text{ and}$$

$$v_t = \left( \frac{G}{\rho} \right)^{1/2}.$$

In this context, *h* is, Planck, $k_B$ is Boltzmann constants, $N_A$ is Avogadro number, $\rho$ is the mass density, *M* is the molecular weight, *n* is the number of atoms per unit cell, $V_l$, $V_t$ and $V_m$ are the longitudinal, transverse and average sound wave velocities, respectively. The calculated $V_l$, $V_t$, $V_m$ and $\theta_D$ for KBeF$_3$ and RbBeF$_3$ are listed in table 3. The Debye temperature indicates the temperature at which atomic vibrations in a crystal lattice become large enough to weaken interatomic bonds and reduce the stiffness of the material. So, materials with greater Debye temperatures are rigid because higher temperatures are
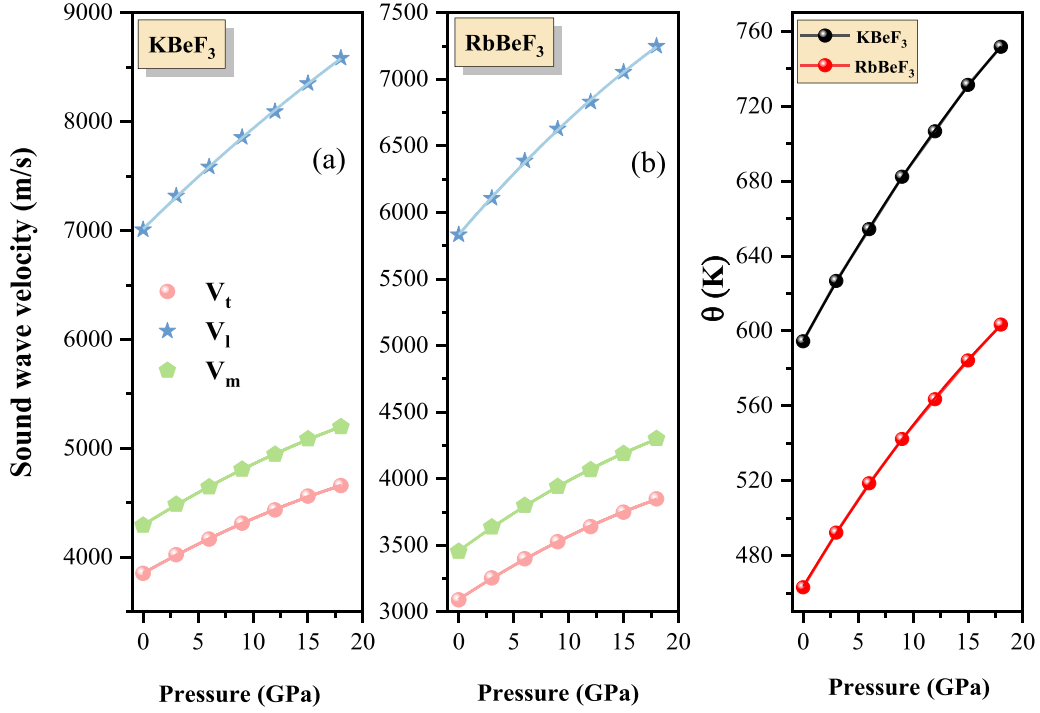
**Figure 6.** Variations of Debye temperature ($\theta_D$) and isotropic longitudinal ($V_l$), transverse ($V_t$), and average ($V_m$) sound velocities as functions of pressure for (a) KBeF$_3$ and (b) RbBeF$_3$.

**Table 4.** Calculated shear anisotropic factors $A_i$ ($i = 1$–3), anisotropy in shear ($A_G$), anisotropy in compression ($A_B$), universal anisotropy index ($A^U$) of XBeF$_3$ (X = K, Be).

| Compounds | $A_1$ | $A_G$ | $A_B$ | $A^U$ |
|---|---|---|---|---|
| KBeF$_3$ | 5.053 | 28% | 0 | 3.91 |
| RbBeF$_3$ | 7.70 | 41% | 0 | 7.00 |

required to break the forces of interatomic bonding and diminish rigidness. However, materials with lower Debye temperatures are more malleable and more deformable because their interatomic bondings are weaker and easily broken. According to the computed elastic moduli values, KBeF$_3$ is stiffer than RbBeF$_3$. Because of the difference in strength between these materials, the Debye temperature of KBeF$_3$ is somewhat greater than that of RbBeF$_3$.

Figure 6 shows the calculated values for $V_l$, $V_t$, $V_m$ and $\theta_D$ of KBeF$_3$ and RbBeF$_3$ under the fixed pressures: 0, 3, 6, 12, 15, and 18 GPa. As KBeF$_3$ is somewhat harder than RbBeF$_3$, the values of Debye temperature and sound speed of KBeF$_3$ are somewhat greater than those of RbBeF$_3$. Variations of Debye temperature $\theta_D$ and sound speed with pressure are well-fitted to the following second-order polynomial:

$$\text{KBeF}_3 \begin{cases} v_t = 3854.87 + 56.77P - 0.66P^2 \\ v_l = 7015.83 + 98.84P - 0.66P^2 \\ v_m = 4297.06 + 63.08P - 0.71P^2 \\ \theta_D = 594.83 + 10.66P - 0.10P^2 \end{cases}$$

$$\text{RbBeF}_3 \begin{cases} v_t = 3093.61 + 54.43P - 0.70P^2 \\ v_l = 5833.99 + 96.12P - 0.98P^2 \\ v_m = 3457.43 + 60.56P - 0.77P^2 \\ \theta_D = 463.67 + 9.71P - 0.11P^2 \end{cases}.$$

*3.2.3. Elastic anisotropy.* Many mechano-physical properties rely heavily on elastic anisotropy, encompassing distinctive phonon modes, phase transformations, dynamics of dislocations, anisotropic plastic deformation, elastic instability, internal friction, and so on [58]. Thus, it becomes crucial to estimate the crystal's degree of elastic anisotropy. Some metrics have been developed to evaluate the degree of elastic anisotropy, such as universal anisotropic index, shear and bulk anisotropy factors, anisotropic shear parameters, and 3D representations of the crystal direction dependence of the elastic moduli.

(i) The universal anisotropic index $A^U$, defined as [59]: $A^U = \frac{5G_V}{G_R} + \frac{B_V}{B_R} - 6$, is widely used to characterize the elastic anisotropy in crystals. For an isotropic crystal, $A^U$ is zero. Thus, the degree of deviation of $A^U$ from zero mirrors the extent of the elastic anisotropy in the crystal [60]. The calculated values of $A^U$ (see table 4) suggest that the title compounds are strongly elastically anisotropic.

(ii) Ranganathan and Ostoja-Starzewski [59] proposed the bulk anisotropy percent $A_B$ ($A_B = \frac{B_V - B_R}{B_V + B_R} \times 100$) and shear anisotropy percent $A_G$ ($A_G = \frac{G_V - G_R}{G_V + G_R} \times 100$) as metrics to evaluate the anisotropy in the bulk modulus and shear modulus, respectively. Note that $B_V$ ($G_V$) and $B_R$ ($G_R$) are the values of $B$ ($G$) according to Voigt and Reuss

approximations. For an isotropic crystal $A_G$ and $A_B$ are equal to zero percent. For a cubic structure, the bulk modulus is isotropic, thus $A_B$ is always equal to zero. The calculated shear modulus percent is equal to 28% in KBeF$_3$ and 41% in RbBeF$_3$, highlighting their strong elastic anisotropy.

(iii) The anisotropic shear parameters $A_1$ ($A_1 = \frac{4C_{44}}{C_{11}+C_{33}-2C_{13}}$), $A_2$ ($A_2 = \frac{4C_{55}}{C_{22}+C_{33}-2C_{23}}$) and $A_3$ ($A_3 = \frac{4C_{66}}{C_{11}+C_{22}-2C_{12}}$) along the shear planes {100}, {010} and {001}, respectively, are also used to characterize the elastic anisotropy extent in crystals [61]. For a cubic system $A_1 = A_2 = A_3$. For an isotropic cubic crystal, $A_1$ is equal to unity. Therefore, the degree of elastic anisotropy can be evaluated from the degree of deviation of $A_1$ from unity. The calculated value of $A_1$ is about 5 for KBeF$_3$ and about 7 for RbBeF$_3$, highlighting the strong elastic anisotropy of these compounds.

(iv) A very useful approach to evaluate the elastic anisotropy of a crystal is by visualizing the crystal direction dependence of its elastic moduli using the ELATE code [62]. The three-dimensional (3D) representation of the crystal direction dependence of an isotropic elastic modulus will have a perfect spherical shape. Thus, the extent of anisotropy of an elastic modulus can be evaluated from the degree of deviation of the 3D representation of its crystal direction dependence from the spherical shape. Figures 7–9 display the 3D representations of the crystal direction dependence of Young's modulus, shear modulus, and Poisson's ratio, respectively, as well as their cross-sections in the *xy, xz,* and *yz* planes. One notes the strong deviations of the 3D representations (cross-sections) of Young's modulus, shear modulus, and Poisson's ratio from the spherical shape (circular form), highlighting the strong elastic anisotropy of the studied materials. Indeed, there are consistent differences between the maximum and minimum values of these elastic moduli, which highlight their strong elastic anisotropy (see table 5). The minimum value of Yung's modulus ($E_{\min}$) appears along the $<100>$ direction and is 54.8 GPa (35.5 GPa) and le maximum value ($E_{\max}$) occurs along the $<111>$ direction and is 223.8 GPa (215.6 GPa) for KBeF$_3$ (RbBeF$_3$). The shear modulus exhibits a maximum value ($G_{\max}$) of 98.3 GPa (95.1 GPa) along the $<001>$ direction and a minimum value ($G_{\min}$) of 19.4 GPa (12.3 GPa) along the $<111>$ directions for KBeF$_3$ (RbBeF$_3$). The maximum value of Poisson's ratio ($\sigma_{\max}$) appears along the $<111>$ and the minimum value ($\sigma_{\min}$) appears along the $<100>$ direction.

## 3.3. Thermodynamic properties

Pressure and temperature are essential parameters in understanding the various properties of materials. We studied the thermodynamic properties such as specific heat, bulk modulus, thermal expansion, etc of XBeF$_3$ (X = K, Be). We utilized the Debye quasi-harmonic model which was applied in the Gibbs software [37] to examine the response of these compound's physical properties with pressure and temperature.

The crystal lattice constant ($\alpha$) of KBeF$_3$ and RbBeF$_3$ was studied across a wide temperature range up to 1000 K, with various fixed pressures: $P = 0, 4, 8, 12,$ and 16 GPa, as well as pressures $P$ up to 16 GPa under various fixed temperatures $T = 0, 200, 400, 600, 800,$ and 1000 K, are displayed in figure 10. Due to the contrasting effects of temperature and pressure on the crystal lattice constant $\alpha$, it heightens as the temperature rises and decreases as the pressure increase. Our calculations indicate that at zero pressure and at a temperature of 300 K, the lattice parameter is 3.6999 Å for KBeF$_3$ and 3.8144 Å for RbBeF$_3$.

Figure 11 demonstrates the evolution of the bulk modulus with the impact of pressure and temperature. It was observed that the coefficient compressibility decreases as the temperature increases and increases with increasing pressure. At $P = 0$ GPa and $T = 300$ K, the $B$ value for KBeF$_3$ is 98.025 GPa and 93.97 GPa for RbBeF$_3$.

The differences in thermal expansion due to pressure and temperature are depicted in figure 12. For temperatures below 300 K, the coefficient of thermal expansion exhibits a rapid increase as the temperature rises, followed by a more moderate increase at higher temperatures. At $P = 0$ GPa and $T = 300$ K, the coefficient of thermal expansion of KBeF$_3$ is $7.77 \times 10^{-5}$ K$^{-1}$, and for RbBeF$_3$ is $8.20 \times 10^{-5}$ K$^{-1}$.

The isochoric heat capacity ($C_V$) with temperature at specific constants pressure ($P = 0, 4, 8, 12,$ and 16 GPa) and with pressures $P$ up to 16 GPa under fixed temperatures ($T = 0, 200, 400, 600, 800,$ and 1000 K) are illustrated in figure 13. From 0 to 400 K, $C_V$ increases exponentially and sharply because of the increment of atomic vibrations. As the temperature rises, the heat capacity values ($C_V$) demonstrate a progressive approach to the Dulong–Petit limit, which is approximately (124.66 J·mol$^{-1}$·K$^{-1}$), which is shared by all solids at high temperatures [63, 64]. As the pressure rises, $C_V$ decreases. Note the impact of temperature on the $C_V$ is more noteworthy than that of pressure. At $P = 0$ GPa and $T = 300$ K, $C_V$ is 102.68 J·mol$^{-1}$·K$^{-1}$ and 109. 01 J·mol$^{-1}$·K$^{-1}$ for KBeF$_3$ and RbBeF$_3$ respectively.

The isobaric heat capacity ($C_P$) versus the temperature and pressure are illustrated in figure 14. At lower temperatures ($T < 200$ K) $C_p$ increases faster with increasing temperature, however, at high temperatures, $C_P$ follows a linear increase. For $P = 0$ GPa, $T = 300$ K $C_p$ is 107.75 J·mol$^{-1}$·K$^{-1}$ for KBeF$_3$ and 114.90 J·mol$^{-1}$·K$^{-1}$ for RbBeF$_3$.

Studying the variation of Debye temperature ($\theta_D$) with temperature and pressure helps us to understand the alteration in thermal vibration frequency of particles caused by changes in temperature and pressure. The temperature dependency of the Debye temperature ($\theta_D$) is presented in figure 15. It is observed that the Debye temperature $\theta_D$ remains relatively stable from 0 to 100 K and then decreases linearly as the temperature rises from $T = 200$ K. However, it increases with increasing pressure. The computed $\theta_D$ for KBeF$_3$ and RbBeF$_3$ using the quasi-harmonic Debye model at $P = 0$ GPa and $T = 0$ K are
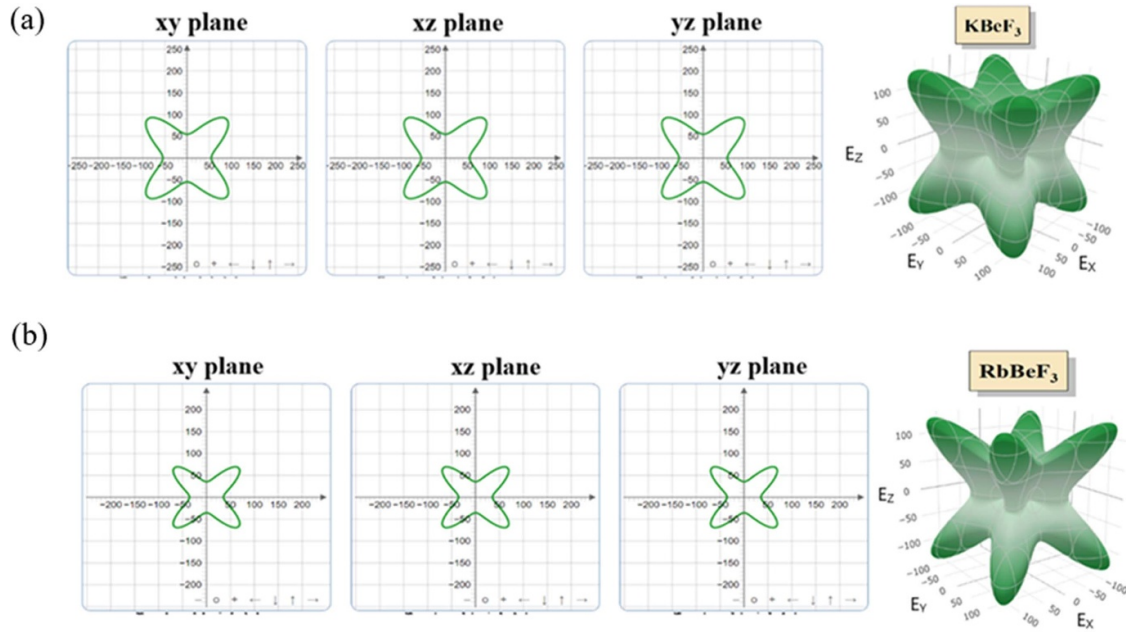
**Figure 7.** 3D and 2D representations of the crystal direction dependence of Young's modulus (*E*) for (a) KBeF$_3$ and (b) RbBeF$_3$.
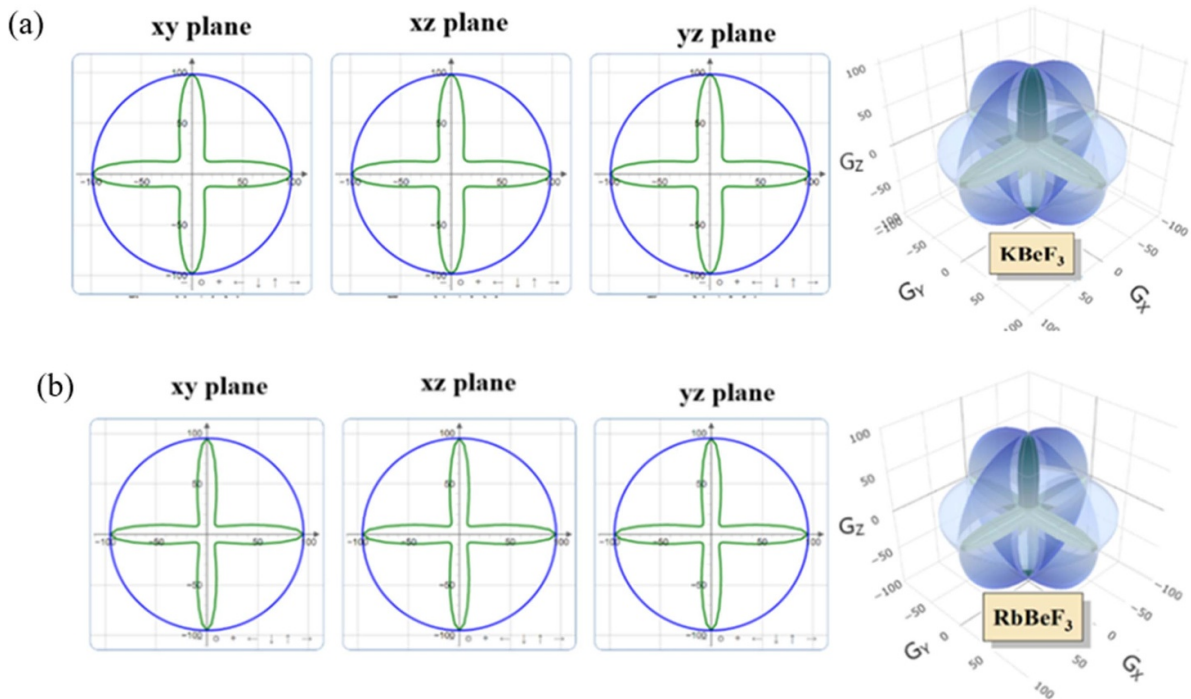


**Figure 8.** 3D and 2D representations of the crystal direction dependence of shear modulus (*G*) for (a) KBeF$_3$ and (b) RbBeF$_3$.

619.19 K and 514.37 K respectively, which are very similar to the corresponding values calculated from the elastic constants.

### 3.4. Electronic properties

The electronic properties of solids pertain to the electronic band structure and density of states (DOS), providing essential information about the behavior of electrons in different states

at each energy level. The metallic, semiconducting, or insulating nature of solid materials is easily understood by studying the electronic features. The band structures of XBeF$_3$ (X = K, Rb) calculated along high symmetry directions *X*–*R*–*M*–Γ–*R* within the cubic BZ are shown in figure 16.

The energy band diagram shows that both the valence band maxima is situated at point *R* in the reciprocal space ($K_x = K_y = K_z = {}^\pi/_a$) and the conduction band minima is situated at point Γ in the reciprocal space ($K_x = K_y = K_z = 0$),
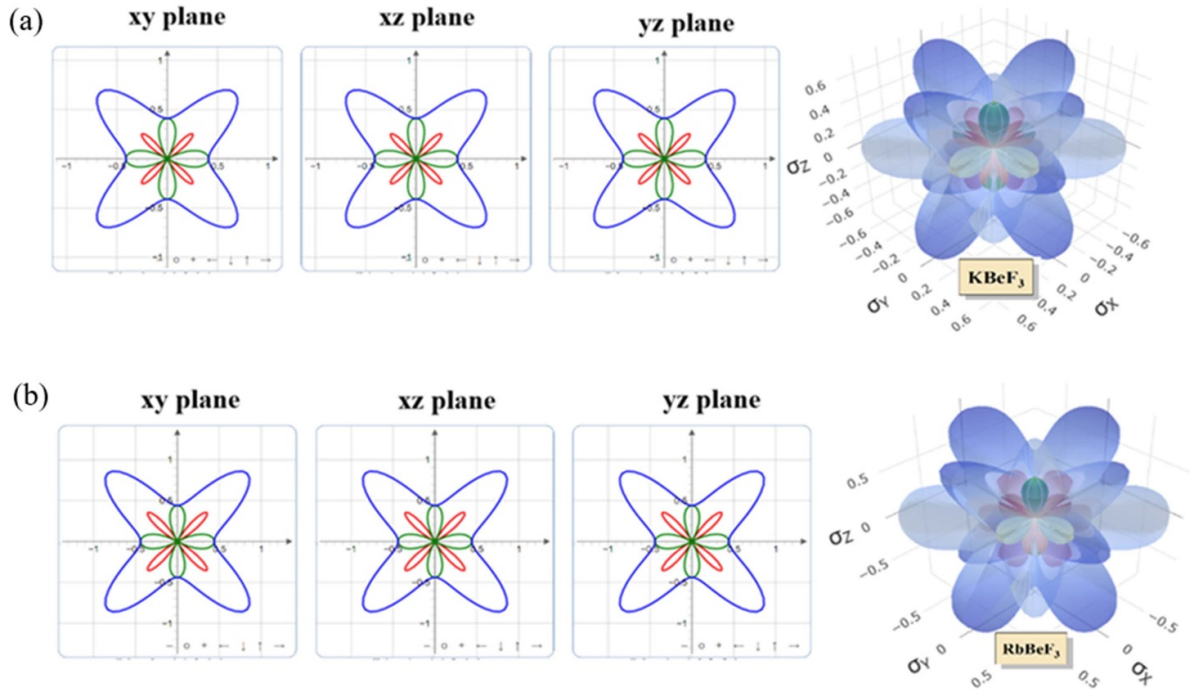
**Figure 9.** 3D and 2D representations of the crystal direction dependence of Poisson's ratio ($\sigma$) for (a) $KBeF_3$ and (b) $RbBeF_3$.

**Table 5.** The minimum and maximum values of young's modulus $E$, shear modulus $G$, and Poisson's ratio $\sigma$ of $KBeF_3$ and $RbBeF_3$.

| Compounds | $E$ (GPa) | | $G$ (GPa) | | $\sigma$ | |
|---|---|---|---|---|---|---|
| | $E_{min}$ | $E_{max}$ | $G_{min}$ | $G_{max}$ | $\sigma_{min}$ | $\sigma_{max}$ |
| $KBeF_3$ | 54.83 | 223.76 | 19.42 | 98.33 | −0.35 | 0.94 |
| $RbBeF_3$ | 35.52 | 215.61 | 12.33 | 95.12 | −0.5 | 1.17 |

confirming that the studied compounds have indirect band gap. The calculated energy band gap value at zero pressure of $KBeF_3$ is 7.99 eV and $RbBeF_3$ is 7.26 eV. The larger band gap ensured the insulating behavior of these materials. The obtained findings are consistent with the previous theoretical results [10, 19, 26, 27, 38].

In order to better understanding of the mechanism of electronic structure, the total and partial electron DOS around the Fermi level which is indicated by the horizontal blue dashed line at 0 eV of $XBeF_3$ (X = K, Rb) at pressures of 0 GPa and 18 GPa in the range of −10–15 eV are presented in figure 17. The TDOS plots are useful for evaluating each cation's participation in the band structure of the studied materials; however, PDOS calculations are more instructive for explaining a lower section of the conduction energy band and upper region of the valence energy band. The valance band edge ranging from 0 to −10 eV exhibits a high DOS in the band structure, whereas the conduction band edge has a lower DOS, indicating that there are more holes at the valence band edge than electrons at the conduction band edge. We have estimated the PDOS of K, Rb, Be and F atoms of compounds $XBeF_3$ (X = K, Rb).

It can be observed that the lowest energy band consists of the K-3p and Rb-4p electronic states electronic states within −10 eV to ∼ −5 eV. The F-2p orbital contributes mainly to the Total DOS at the zero level, and there is also some contribution from the Be-2s state. Therefore, the charge transport and binding characteristics of $XBeF_3$ (X = K, Rb) are likely to be dominated by hybridization among these orbitals, and the higher energy bands are formed by Be-s states with small contributions of K-p and Rb-p states. According to figure 18, the band gap of $XBeF_3$ (X = K, Rb) increases as pressure increases. This effect is due to the diminution in the lattice parameter and in bond lengths of X–F and Be–F as pressure increases. The energy states developed in these bonds increase the Fermi energy, which in turn alters conduction and valence states. And this rise can also be explained by the ionic bonding properties in these compounds, in most cases, increasing pressure on an ionic compound will result in an increase in its band gap ($E_g$). As the ions come closer together, the electrostatic forces between them become stronger, which can lead to an increased energy gap between the valence and conduction bands [65], which is confirmed in figure 19 where the result obtained from the density charge analysis shows the ionic bond between its constituent atoms,

### 3.5. Optical properties

The electrical and optical properties of the material are affected when it interacts with electromagnetic waves, and this
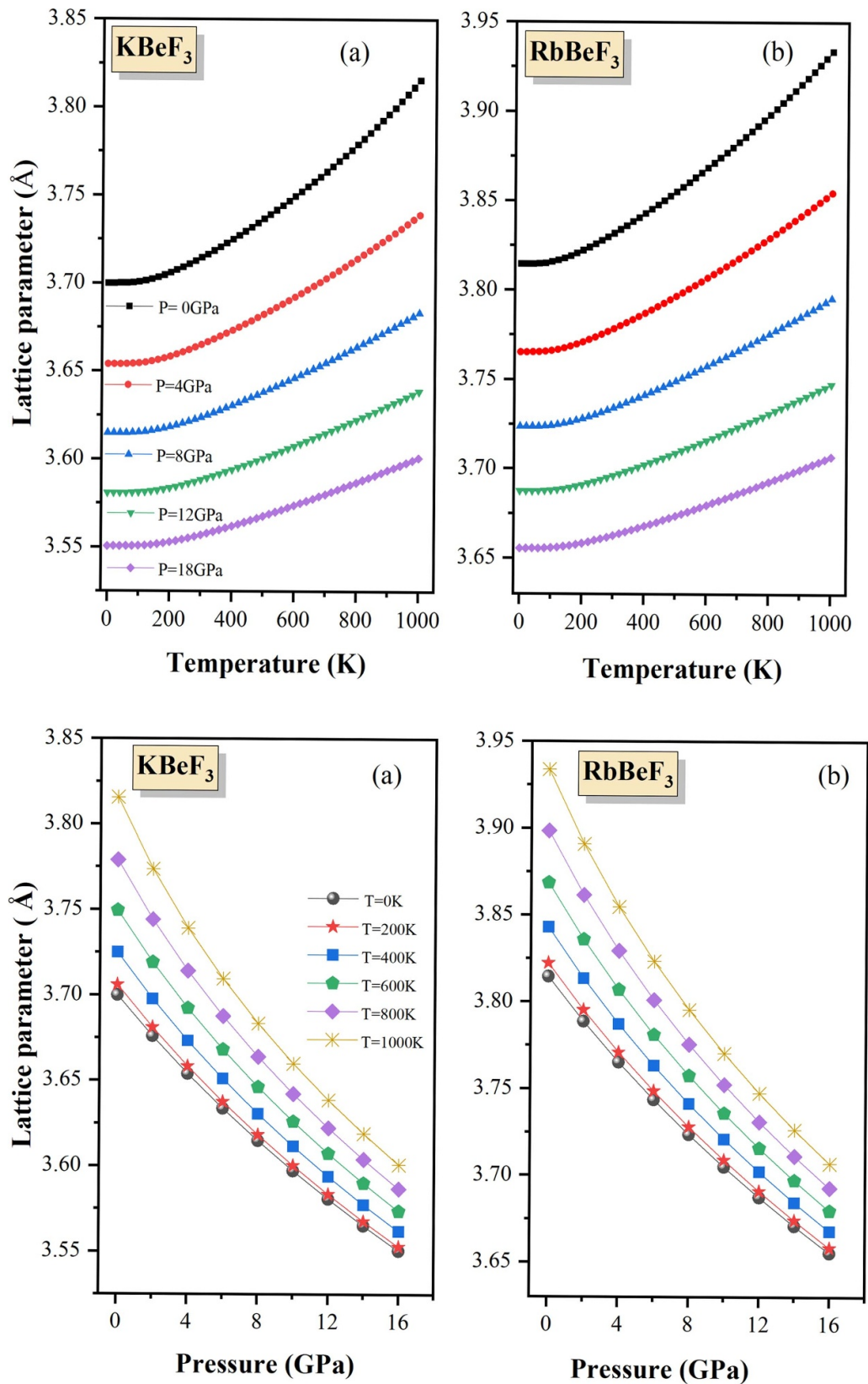
**Figure 10.** Variations of the lattice parameter (*a*) with temperature at constant pressures and with pressure at constant temperatures for (a) KBeF$_3$ and (b) RbBeF$_3$.
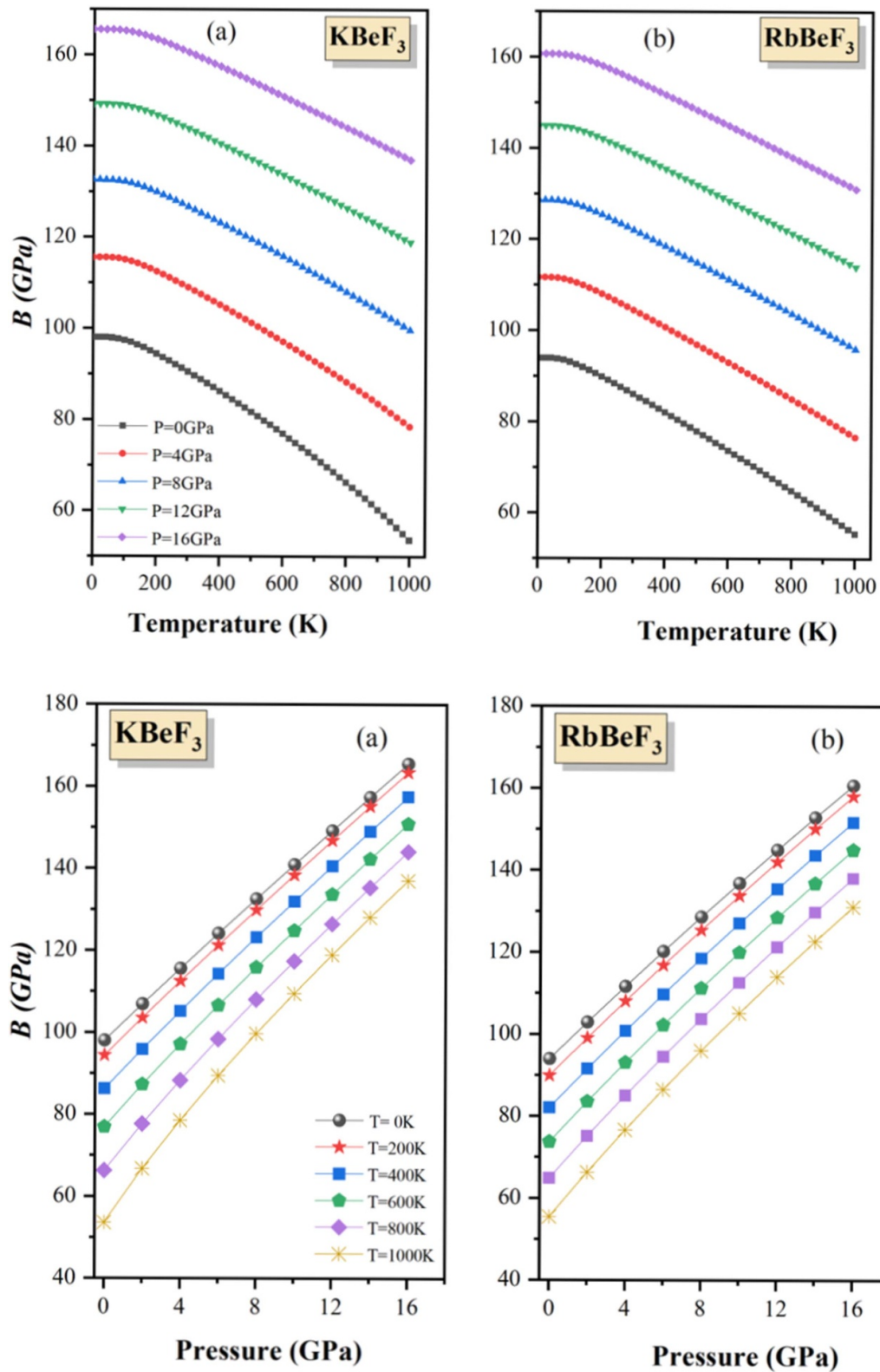
**Figure 11.** Evolutions of the bulk modulus ($B$) of (a) KBeF$_3$ and (b) RbBeF$_3$ with temperature at constant pressures and with pressure at constant temperatures.
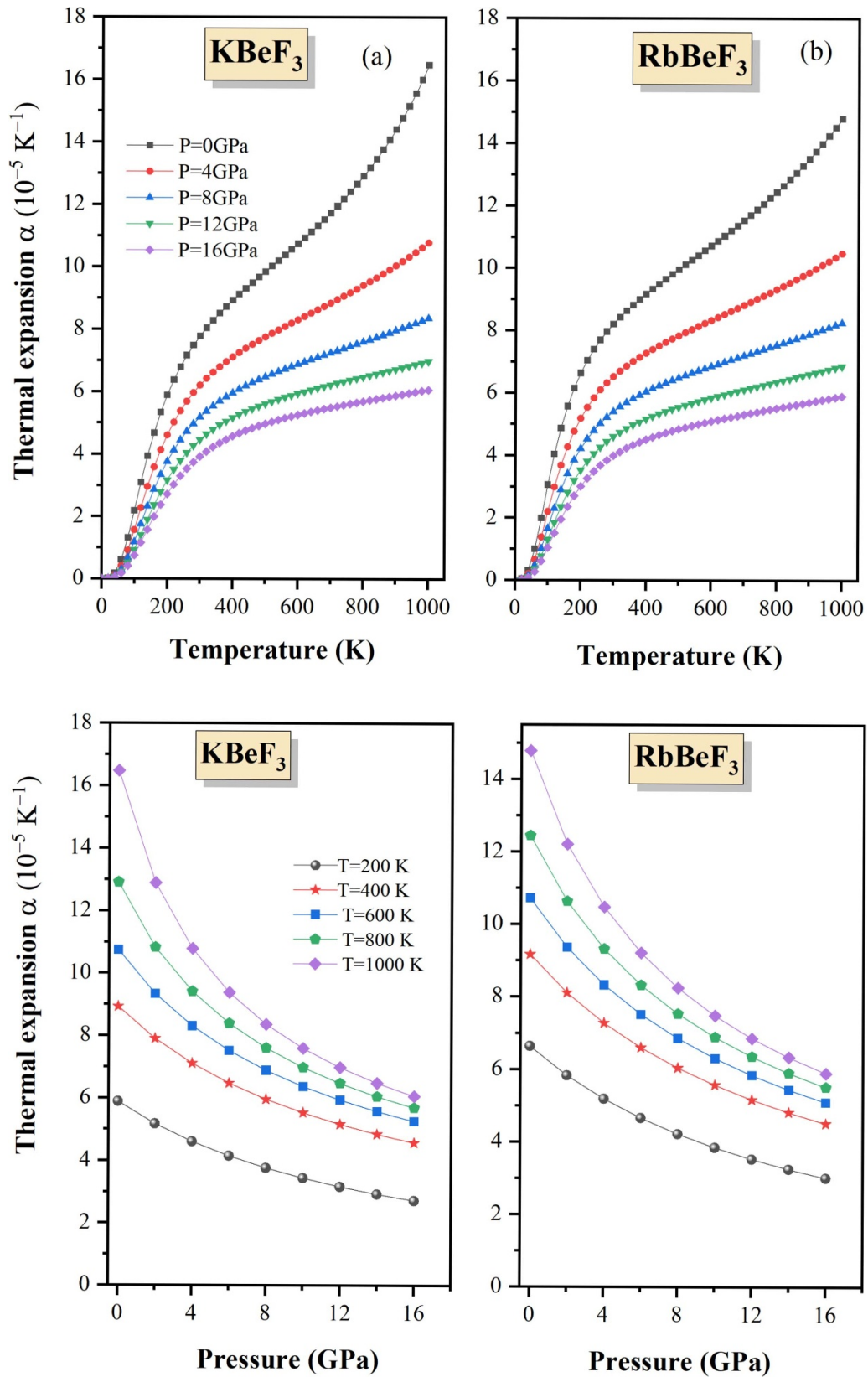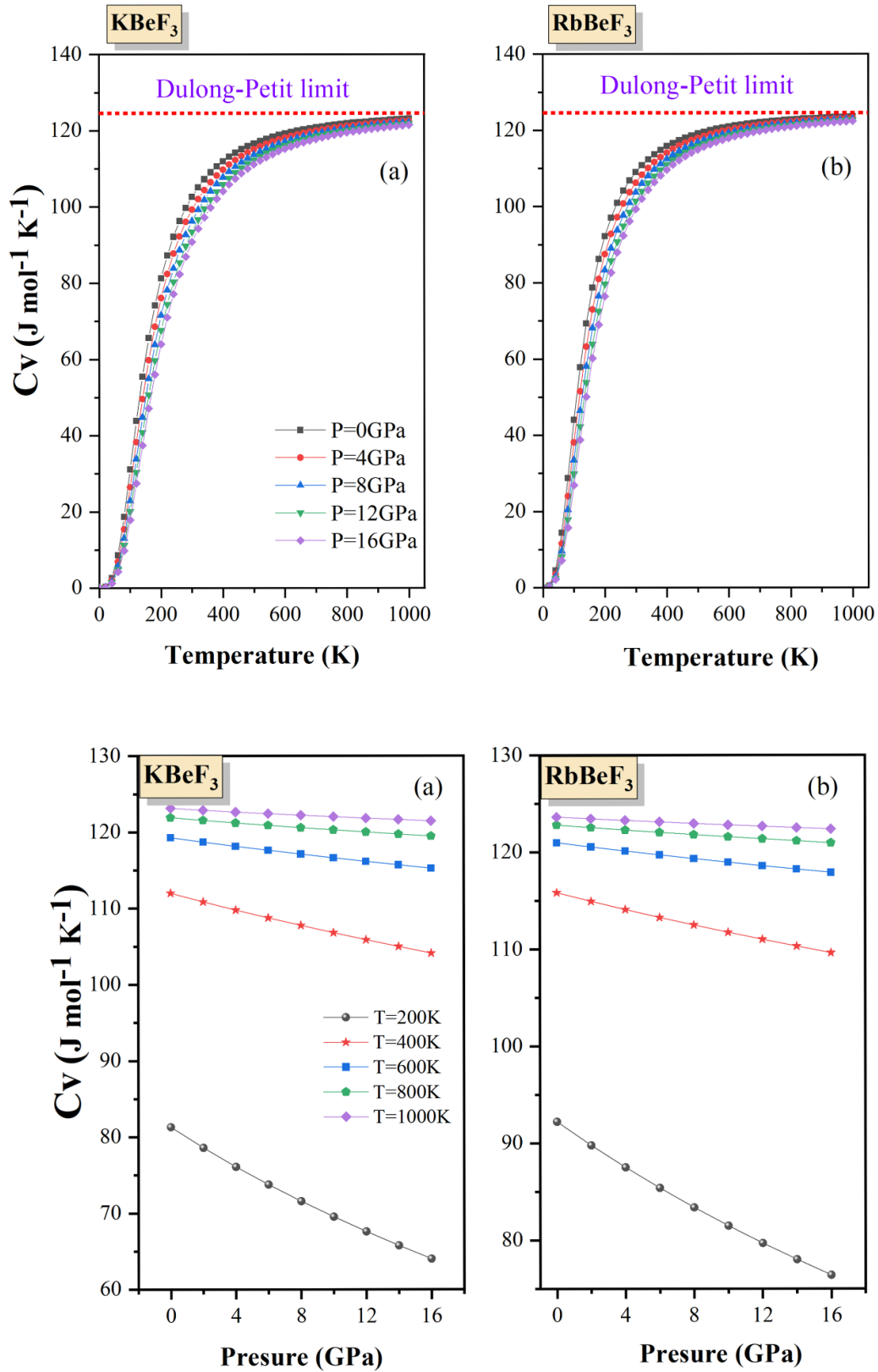
**Figure 12.** Changes in the coefficient of thermal expansion ($\alpha$) with the temperature at constant pressures and with pressure at constant temperatures for (a) KBeF$_3$ and (b) RbBeF$_3$.

**Figure 13.** The variations of isochoric heat capacities ($C_V$) for the perovskites (a) KBeF$_3$ and (b) RbBeF$_3$ with the temperature at constant pressures and with pressure at constant temperatures.
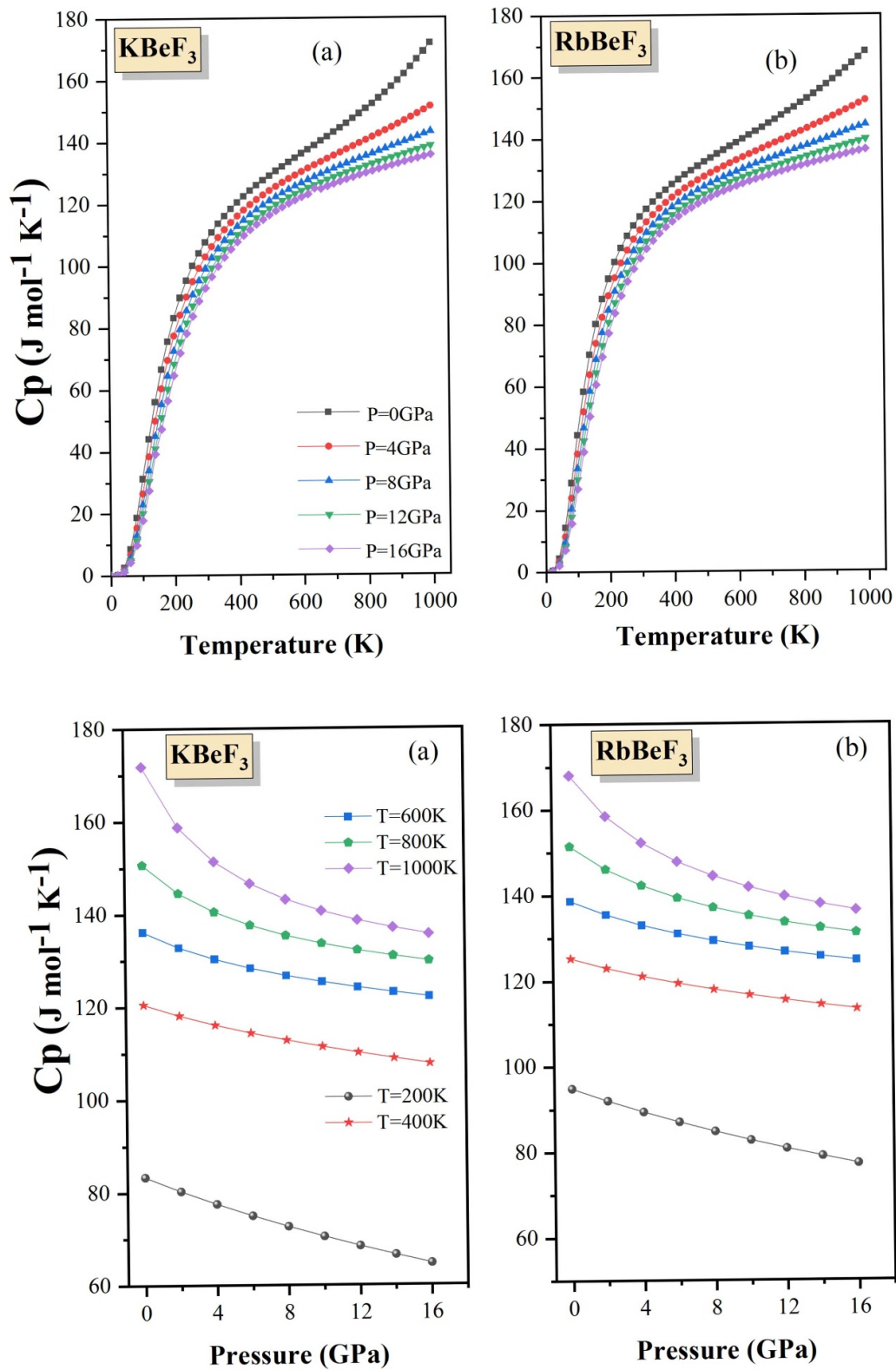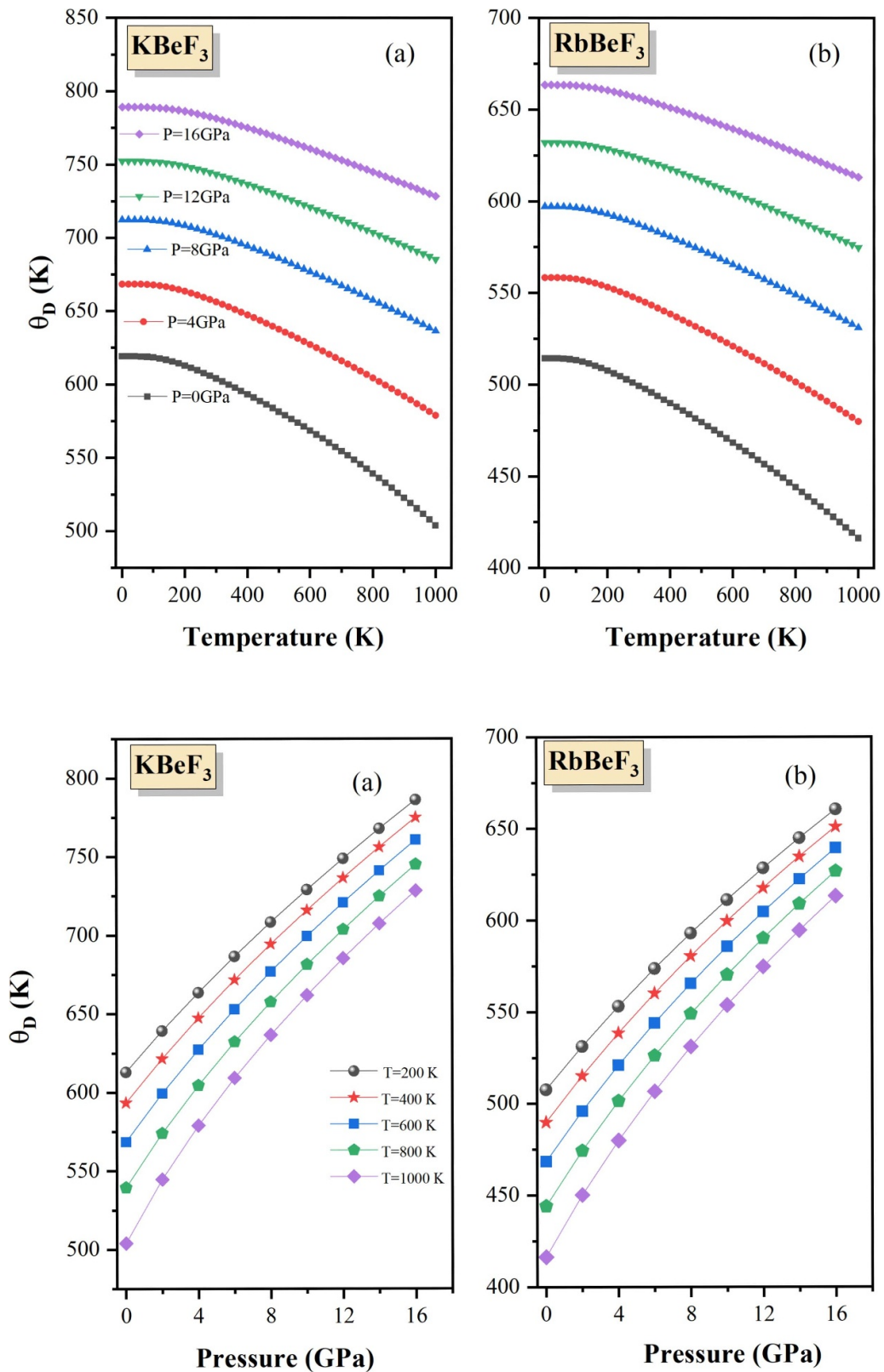
**Figure 14.** The variations of the isobar heat capacities ($C_\mathrm{p}$) for the perovskites (a) KBeF$_3$ and (b) RbBeF$_3$ with the temperature at constant pressures and with pressure at constant temperatures.

**Figure 15.** The variations of the Debye temperature ($\theta_D$) for the perovskites (a) KBeF$_3$ and (b) RbBeF$_3$ with the temperature at constant pressures and with pressure at constant temperatures.
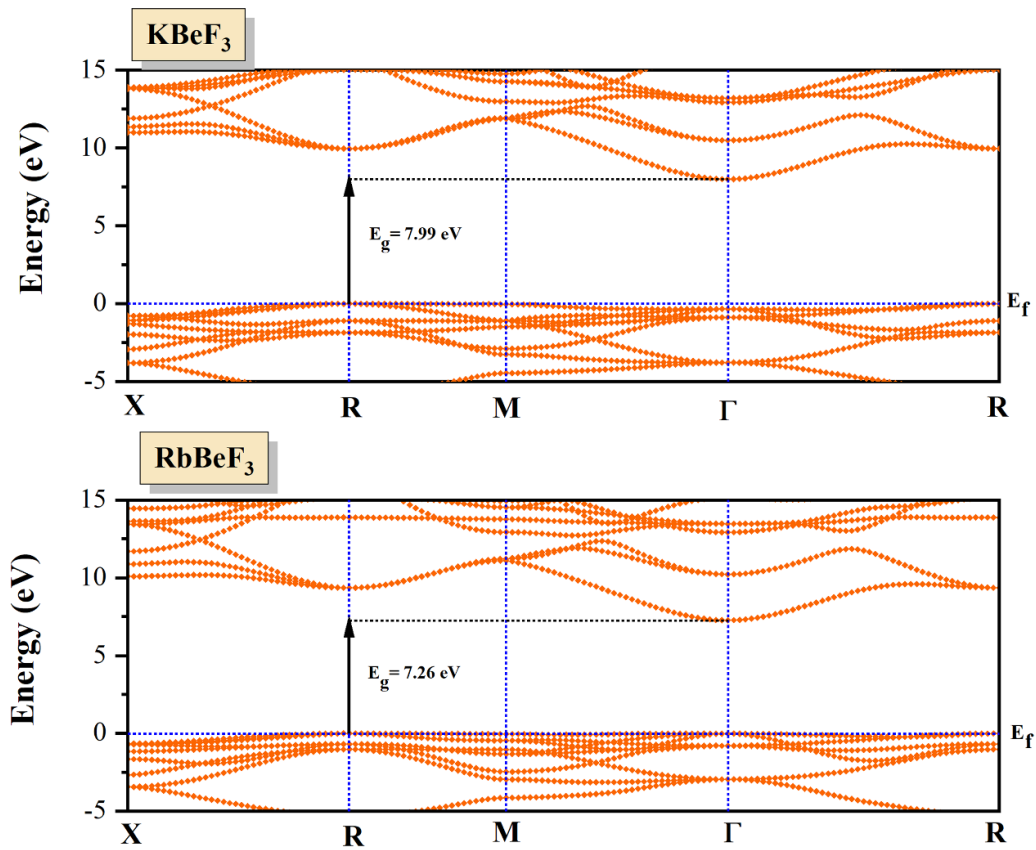
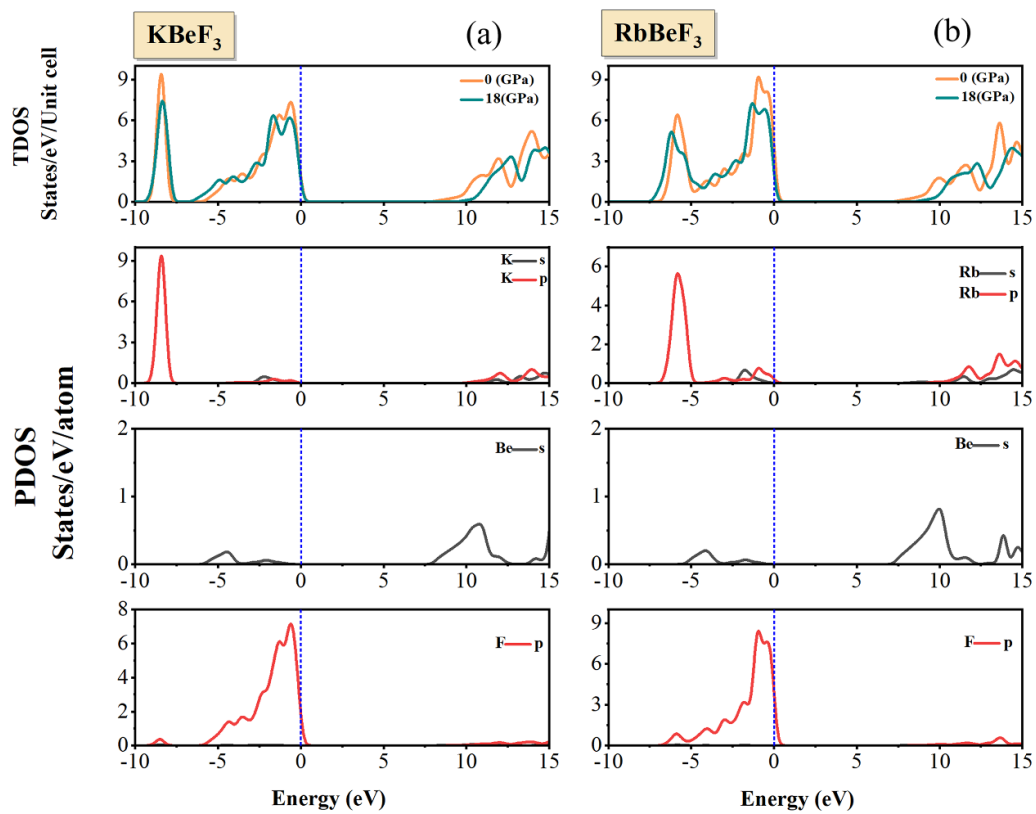**Figure 16.** Electronic band structure of (a) KBeF$_3$ and (b) RbBeF$_3$ compounds.



**Figure 17.** Total and partial DOS of (a) KBeF$_3$ and (b) RbBeF$_3$ compounds.
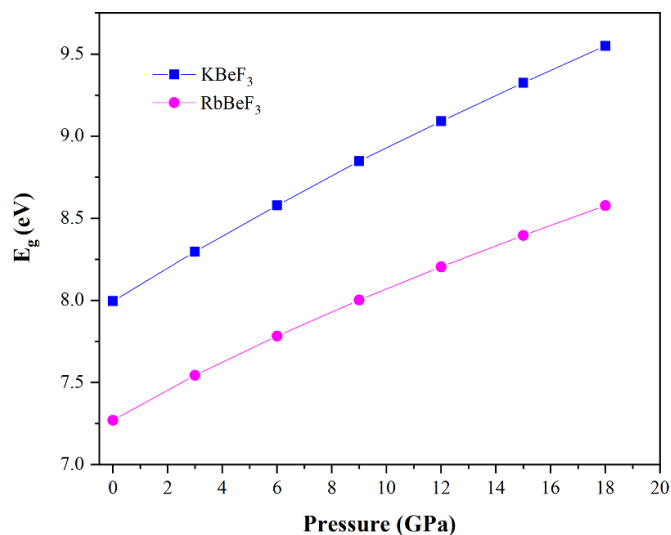
**Figure 18.** The effect of pressure on the energy gap for KBeF$_3$ and RbBeF$_3$ compounds.
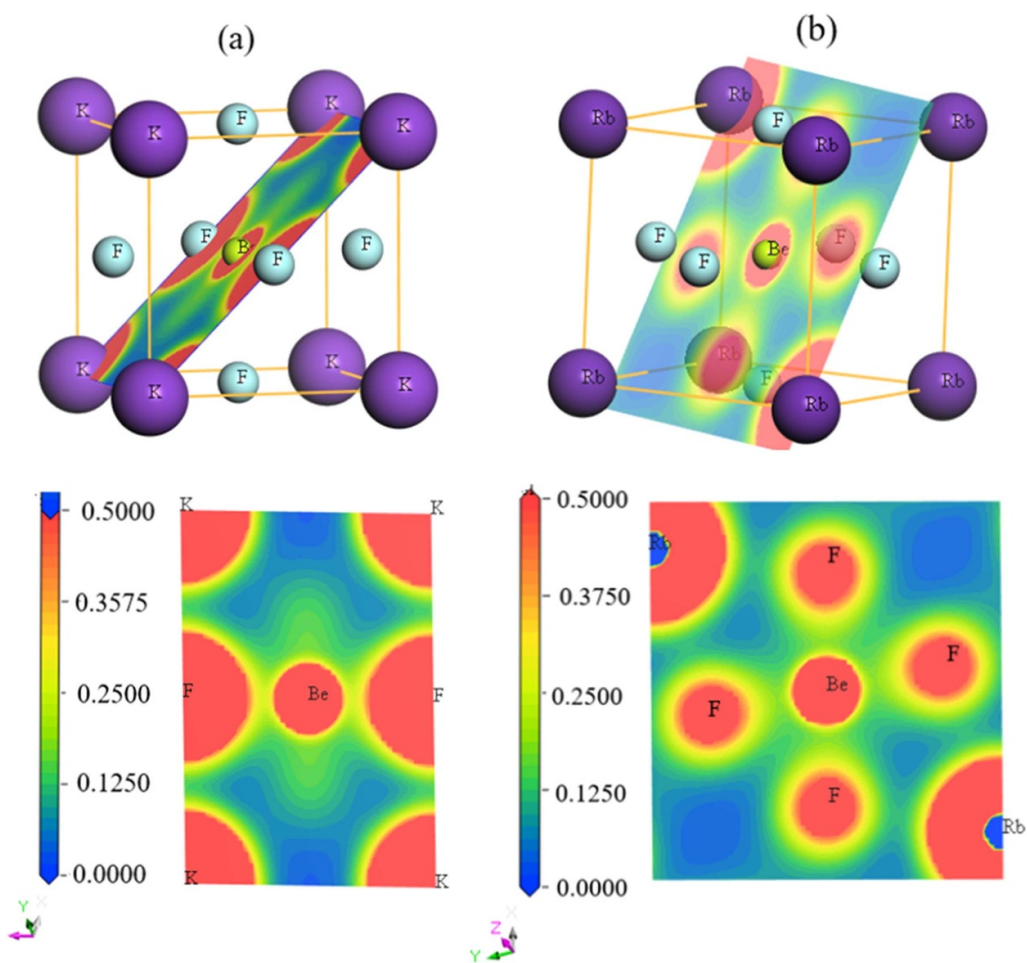


**Figure 19.** Electron charge density distribution of (a) of KBeF$_3$ and (b) RbBeF$_3$ compounds.
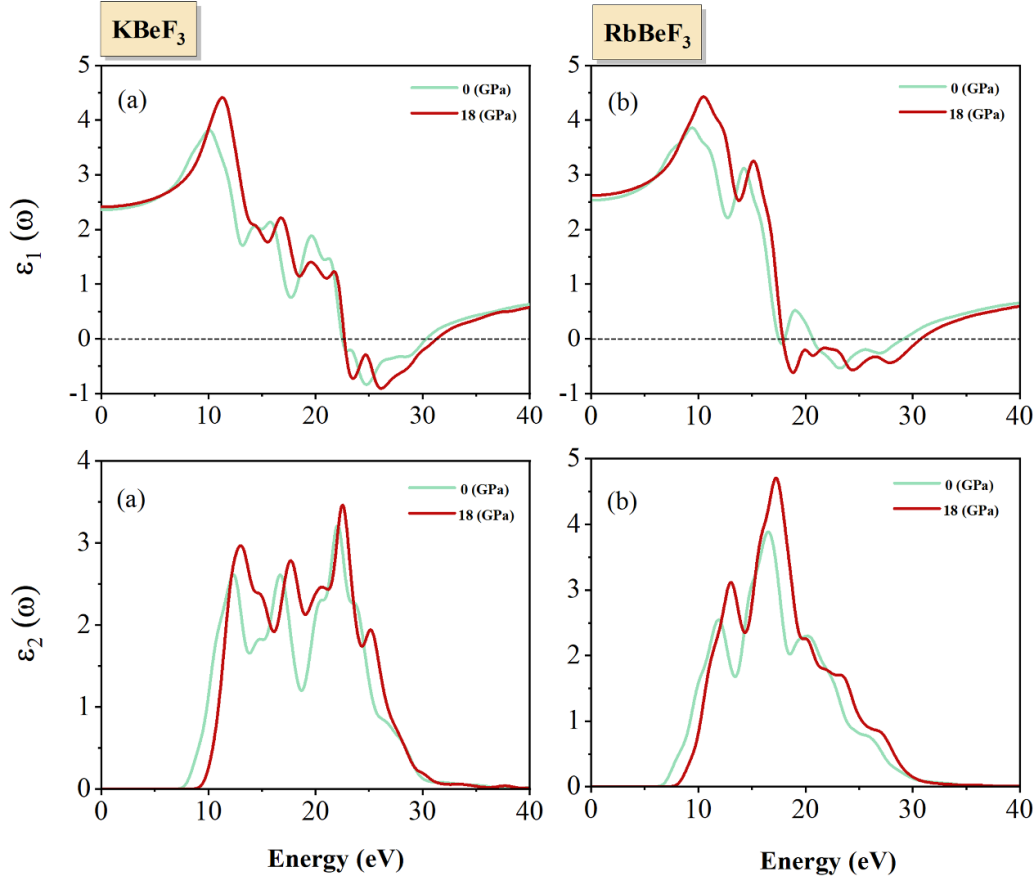
**Figure 20.** Computed imaginary part $\varepsilon_2(\omega)$ and real part $\varepsilon_1(\omega)$ for the (a) KBeF$_3$ and (b) RbBeF$_3$ at 0 and 18 GPa pressure.

is determined by the complex dielectric function $\varepsilon(x)$ that describes its optical properties [66–68]. This function can be written as:

$$\varepsilon(\omega) = \varepsilon_1(\omega) + i\varepsilon_2(\omega)$$

The complex dielectric function ($\varepsilon$) is divided into two parts. Firstly, ($\varepsilon_1$) corresponds to polarization; secondly, ($\varepsilon_2$) expounds on the energy dissipation in the system [69] as illustrated in figure 20. The Kramers–Kronig relationship [70, 71] can be used to obtain the real part

$$\varepsilon_1(\omega) = 1 + \frac{2}{\pi} P \int_0^\infty \frac{\omega' \varepsilon_2(\omega')}{\omega'^2 - \omega^2} d\omega'$$

where $P$ is the principal value of the integral

$$\varepsilon_2(\omega) = \frac{2e^2\pi}{\Omega \varepsilon_0} \sum_{k,v,c} |\psi_k^c| u.r |\psi_k^v|^2 \delta(E_k^c - E_k^v - E)$$

where subscripts $k$, $\nu$, c represent the reciprocal lattice vector, the conduction band, and the lower valence band, $u, \omega, e, \psi_k^c$, and $\psi_k^v$ are the incident electric field polarization vector, light frequency, electronic charge, and conduction and valence band wave functions at $k$, respectively, and $E_k^c$ and $E_k^v$ are intrinsic energy levels.

Optical coefficients, including the refractive index $n(\omega)$, extinction coefficient $k(\omega)$, absorption coefficient $\alpha(\omega)$, reflectivity $R(\omega)$, and energy loss coefficient $L(\omega)$ can be determined from the dielectric function using the following relations [52, 72, 73]

$$n(\omega) = \left( \sqrt{\varepsilon_1^2(\omega) + \varepsilon_2^2(\omega)} + \varepsilon_1(\omega) \right)^{\frac{1}{2}} \bigg/ \sqrt{2}$$

$$k(\omega) = \left( \sqrt{\varepsilon_1^2(\omega) + \varepsilon_2^2(\omega)} - \varepsilon_1(\omega) \right)^{\frac{1}{2}} \bigg/ \sqrt{2}$$

$$\alpha(\omega) = \sqrt{2}\omega \left( \sqrt{\varepsilon_1^2(\omega) + \varepsilon_2^2(\omega)} - \varepsilon_1(\omega) \right)^{\frac{1}{2}}$$

$$R(\omega) = \left| \frac{\varepsilon(\omega)^{1/2} - 1}{\varepsilon(\omega)^{1/2} + 1} \right|^2$$

$$L(\omega) = \frac{\varepsilon_2(\omega)}{\varepsilon_1^2(\omega) + \varepsilon_2^2(\omega)}.$$

The figures 20–22 show the predicted optical properties for the polarization direction [100] at the equilibrium lattice constant within the energy range of 40 eV. The most essential quantities for the real dielectric function are the zero-frequency limit $\varepsilon_1(0)$, with values of 2.36 eV (2.53 eV) at
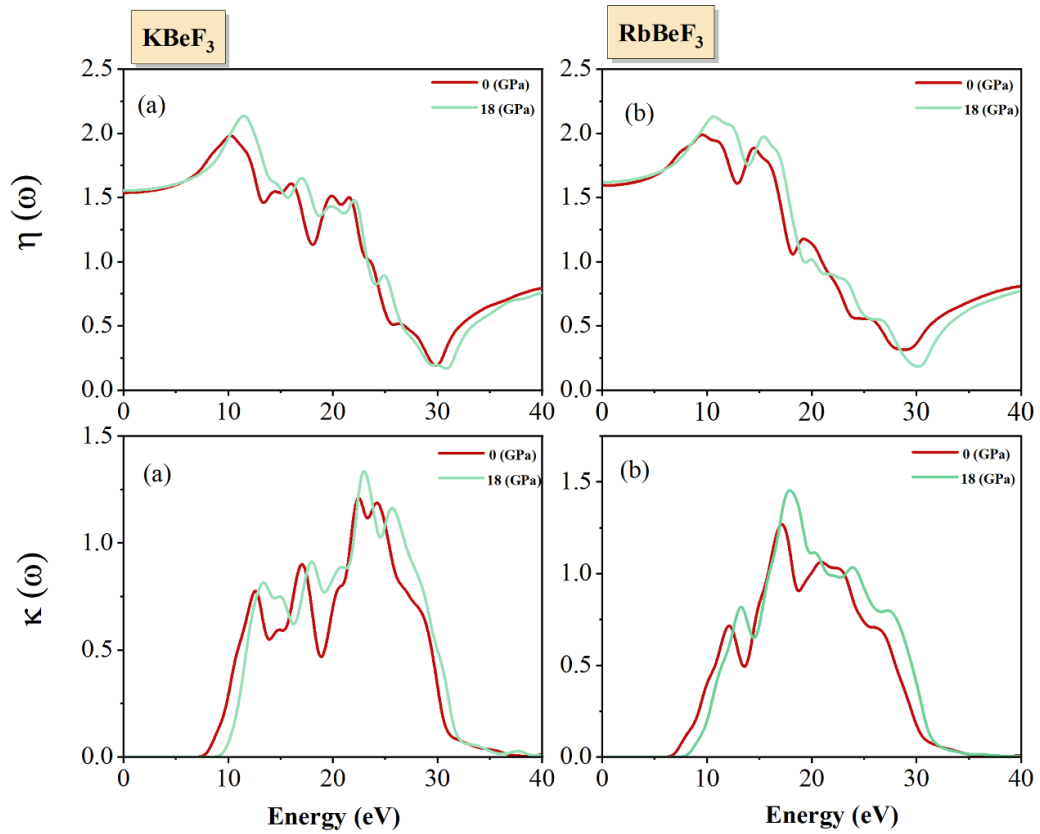
**Figure 21.** Computed refractive index $\eta\,(\omega)$ and extinction coefficient $\kappa\,(\omega)$ for the (a) KBeF$_3$ and (b) RbBeF$_3$ compounds.
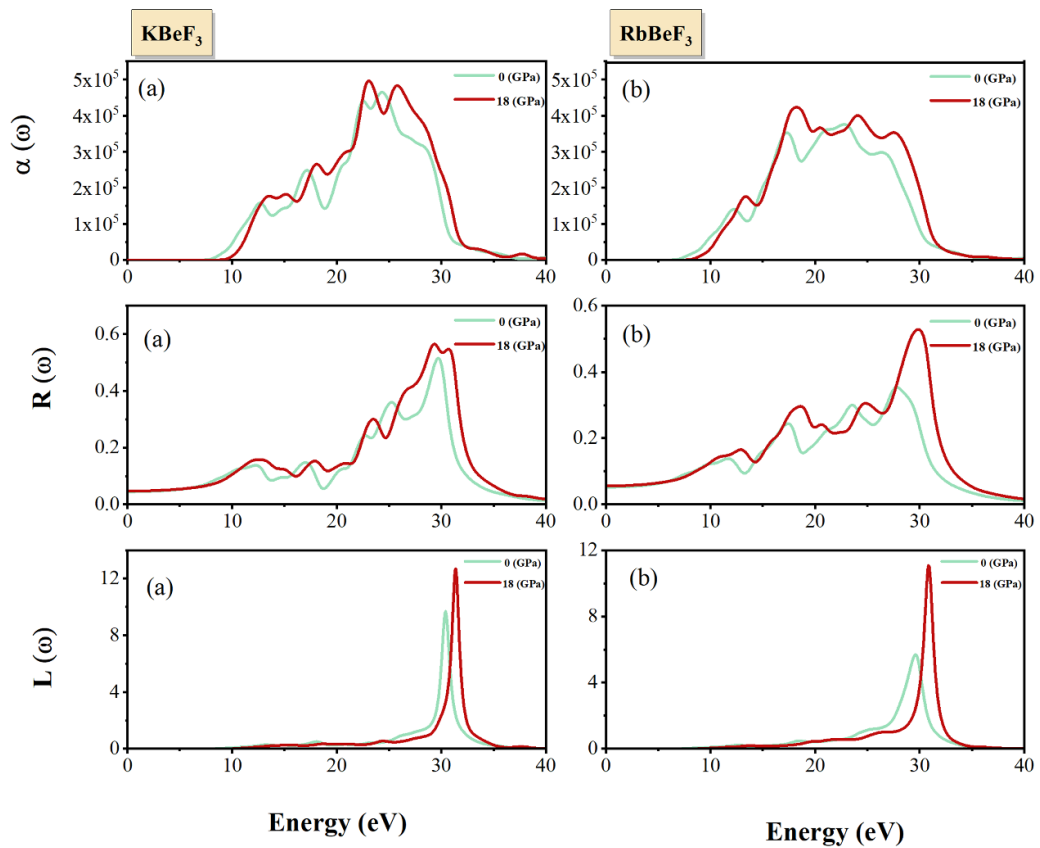


**Figure 22.** Computed optical constants for the (a) KBeF$_3$ and (b) RbBeF$_3$ compounds: absorption, reflectivity, and energy-loss spectrum.

$P = 0$ GPa, and 2.41 eV (2.62 eV) for KBeF$_3$ (RbBeF$_3$). Note that these values increase with increasing pressure. Then $\varepsilon_1$ becomes negative. This means that these compounds behave like metals due to energy loss and poor light transmission through the material with substantial reflection [74]. The dielectric function imaginary part is related directly to the energy of the band gap. Looking more closely at the $\varepsilon_2(\omega)$ patterns, we find that the initial critical point is around 7.9 eV and 6.97 eV for KBeF$_3$ and RbBeF$_3$, respectively.

These observed values are consistent with an indirect transition among VB and CB at point ($R$–$\Gamma$) for KBeF$_3$ and RbBeF$_3$. At 0 GPa, $\varepsilon_2(\omega)$ shows three main peaks at 12.3, 16.6, and 22 eV, corresponding to the three absorption. This indicates significant behavior of absorption at these energy ranges and hence more appropriate for UV optoelectronic applications.

Calculate the extinction coefficient $k$ and refractive index $\eta$ as shown in figure 21. As shown in the refractive index spectrum, the constant refractive index $\eta$ (0) which indicates the refractive index at zero eV, is 1.53 and 1.59 for KBeF$_3$ and RbBeF$_3$, respectively. At photon energy of 10.13 eV, KBeF$_3$ has the greatest refractive index peak of 1.98, whereas RbBeF$_3$ has a highest refractive index peak of 1.99 at 9.55 eV photon energy. The refractive index value may be used to calculate that how much is the refracted light from any material, and is helpful in the applications of photoelectric. Owing to the photon's interaction with the electron, we can see in figure 21 that the photon faces an obstacle when entering the compound. The higher the value of $\eta$ for any material (i.e. $\eta > 1$), then much photons are deflected as they pass through it.

The absorption coefficient indicates data about the optimal efficiency of the conversion of solar energy and expresses the amount of light of certain energy that may penetrable a material before being soaked up. According to figure 22, the coefficient of absorption at zero pressure begins at 8.15 eV (7.35 eV) for KBeF$_3$ (RbBeF$_3$) which becomes equal for the band gap electronic. For KBeF$_3$ and RbBeF$_3$ at 0 GPa, the highest peaks are located at 464 805 cm$^{-1}$ at 24.4 eV and of 375 581 cm$^{-1}$ at 22.7 eV, respectively. In this study, we have seen that XBeF$_3$ (X = K, Rb) materials possess a good coefficient of absorption within the high range of energy. This shows and affirms that these materials have the potential to serve as appropriate candidates for optoelectronic devices functioning in the UV range.

Reflectivity is another important optical property, as it depends on the amount of light reflected by a substance when exposed to it and mainly depends on the incident photon energy on the surface [75]. From the figure 22, we have observed that the reflectance of KBeF$_3$ (RbBeF$_3$) at 0 and 18 GPa starts from a value of 0.04 (0.05) and remains constant in the energy range of visible. Then, under zero GPa pressure, the reflectivity of KBeF$_3$ increases unless it attain its higher value of 0.51 at approximately 29.6 eV, while RbBeF$_3$ exhibits a reflectivity of 0.35 around 27.7 eV. However, under 18 GPa, the reflectivity of KBeF$_3$ reaches 0.56 around 29.3 eV, and RbBeF$_3$ exhibits a reflectivity of 0.52 around 29.8 eV. Following that, the reflectance reduced once again, suggesting that the studied materials had a less energy area, particularly

in the range of visible & infrared, implying that the materials display transparency within these states, making them suitable for applications such as anti-reflective coatings.

A compound's loss function shows the energy lost whenever electrons in any material moves very fast through that material. Figure 22 illustrates the loss functions for KBeF$_3$ and RbBeF$_3$ compounds. The bulk plasma frequency $\omega_P$ is the point at which energy loss seems to be the greatest, and it preserves the following requirements [76, 77] $\varepsilon_2 < 1$ and $\varepsilon_1 = 0$. At zero pressure, the predicted bulk plasma frequencies for KBeF$_3$ and RbBeF$_3$ are 30.27 and 29.61 eV, respectively. This study validated the insulating properties of these materials.

## 4. Conclusion

In the present study, the structural, elastic, thermodynamic, electronic, and optical properties of the perovskite compounds XBeF$_3$ (X = K, Rb) were investigated using (GGA-PBEsol) approximation. The compute crystal lattice constant agreed well with the previously published values for these compounds. By employing EOS to fit the energy–volume and pressure–volume data and formation enthalpy, the structural stability of fluoroperovskites XBeF$_3$ (X = K and Rb) was confirmed; whereas structural instability is observed from the calculated Goldsmith tolerance factor. According to the computed elastic constants, the materials XBeF$_3$ (X = K, Rb) stay mechanically stable up to 18 GPa. High bulk and Young's moduli of KBeF$_3$ ensured that this phase is more capable to resist plastic deformation and is stiffer than KBeF$_3$. Universal anisotropy factor analysis reveals the elastic anisotropy of compounds XBeF$_3$ (X = K, Rb) where both compounds were found elastically anisotropic. Pugh's criterion and Poisson's ratio demonstrate these compounds are ductile, the temperature and pressure dependence of the crystal lattice constant, bulk modulus, isochoric and isobaric heat capacities, coefficient of thermal expansion, and Debye temperature were computed in the extent of 0–1000 K, while 0–16 GPa utilizing the quasi-harmonic approximation. The insulating nature of XBeF$_3$ (X = K, Rb) is confirmed by examination of its band structure. Furthermore, the outcome of the optical study also indicates that the studied materials have the ability to be applied in UV-absorbing devices. Due to their transparency, these materials can be employed in thin film growth as substrates and in various optoelectronic applications and these compounds are promising candidates for VUV-VUV-transparent lens material. We hope that our study will show a substantial influence on forthcoming research work into the varied properties of comparable materials.

## Data availability statements

The data cannot be made publicly available upon publication because they contain sensitive personal information. The data that support the findings of this study are available upon reasonable request from the authors.

## Conflict of interest

The authors declare that there is no potential conflict of interest.

## ORCID iDs

Sarah Chaba Mouna https://orcid.org/0000-0002-2795-7617
Missoum Radjai https://orcid.org/0000-0002-0313-7155
Md. Atikur Rahman https://orcid.org/0000-0002-9591-3018
Abdelmadjid Bouhemadou https://orcid.org/0000-0002-5139-4172

## References

[1] Sajjad M, Khan U A, Ullah H, Alhodaib A, Amami M, Tirth V and Zaman A 2022 Structural, electronic, magnetic and elastic properties of xenon-based fluoroperovskites XeMF$_3$ (M = Ti, V, Zr, Nb) via DFT studies *RSC Adv.* **12** 27508–16

[2] Zhang F, Mao Y, Park T J and Wong S S 2008 Green synthesis and property characterization of single crystalline perovskite fluoride nanorods *Adv. Funct. Mater.* **18** 103–12

[3] Eibschütz M and Guggenheim H J 1968 Antiferromagnetic-piezoelectric crystals: BaMe$_4$ (M = Mn, Fe, Co and Ni) *Solid State Commun.* **6** 737–9

[4] Berastegui P, Hull S and Eriksson S G 2001 A low-temperature structural phase transition in CsPbF$_3$ *J. Phys.: Condens. Matter* **13** 5077

[5] Daniels R R, Margaritondo G, Heaton R A and Lin C C 1983 Experimental study of the electronic structure of KMgF$_3$ *Phys. Rev.* B **27** 3878

[6] Julliard J and Nouet J 1975 Analyse radiocristallographique de la distorsion magnétostrictive dans les antiferromagnétiques KCof$_3$, RbCof$_3$ et TlCof$_3$ *Revue de Physique Appliquée* **10** 325–9

[7] Hua R, Lei B, Xie D and Shi C 2003 Synthesis of the complex fluoride LiBaF$_3$ and optical spectroscopy properties of LiBaF$_3$: M (M = Eu, Ce) through a solvothermal process *J. Solid State Chem.* **175** 284–8

[8] Joshi T K, Shukla A, Sharma G and Verma A S 2020 Computational determination of structural, electronic, optical, thermoelectric and thermodynamic properties of hybrid perovskite CH$_3$CH$_2$NH$_3$GeI$_3$: an emerging material for photovoltaic cell *Mater. Chem. Phys.* **251** 123103

[9] Hörsch G and Paus H J 1986 A new color center laser on the basis of lead-doped KMgF$_3$ *Opt. Commun.* **60** 69–73

[10] Nishimatsu T, Terakubo N, Mizuseki H, Kawazoe Y, Pawlak D A, Shimamura K and Fukuda T 2002 Band structures of perovskite-like fluorides for vacuum-ultraviolet-transparent lens materials *Jpn. J. Appl. Phys.* **41** L365

[11] Ahmed D A, Bağcı S, Karaca E and Tütüncü H M 2018 Elastic properties of ABF$_3$ (A: Ag, K, and B: Mg, Zn) perovskites *AIP Conf. Proc.* **2042** 020035

[12] Dotzler C, Williams G V M and Edgar A 2008 Radiation-induced optically and thermally stimulated luminescence in RbCdF$_3$ and RbMgF$_3$ *Curr. Appl. Phys.* **8** 447–50

[13] Mubarak A A and Mousa A A 2012 The electronic and optical properties of the fluoroperovskite BaXF$_3$ (X = Li, Na, K, and Rb) compounds *Comput. Mater. Sci.* **59** 6–13

[14] Sahnoun M, Zbiri M, Daul C, Khenata R, Baltache H and Driz M 2005 Full potential calculation of structural, electronic and optical properties of KMgF$_3$ *Mater. Chem. Phys.* **91** 185–91

[15] Shimamura K, Fujita T, Sato H, Bensalah A, Sarukura N and Fukuda T 2000 Growth and characterization of KMgF$_3$ single crystals by the Czochralski technique under CF$_4$ atmosphere *Jpn. J. Appl. Phys.* **39** 6807

[16] Yamanoi K, Nishi R, Takeda K, Shinzato Y, Tsuboi M, Luong M V and Ishikawa T 2014 Perovskite fluoride crystals as light emitting materials in vacuum ultraviolet region *Opt. Mater.* **36** 769–72

[17] Ouenzerfi R E, Ono S, Quema A, Goto M, Sarukura N, Nishimatsu T and Fukuda T 2004 Design proposal of light emitting diode in vacuum ultraviolet based on perovskite-like fluoride crystals *Jpn. J. Appl. Phys.* **43** L1140

[18] El Ouenzerfi R, Ono S, Quema A, Goto M, Sakai M, Sarukura N and Fukuda T 2004 Design of wide-gap fluoride heterostructures for deep ultraviolet optical devices *J. Appl. Phys.* **96** 7655–9

[19] Syrotyuk S V and Shved V M 2015 The GW electronic structure of cubic RbMF$_3$ perovskites (M = Be, Mg, Ca, Sr, Ba) *Eur. Phys. J.* B **88** 1–8

[20] Cui S, Feng W, Hu H, Feng Z and Wang Y 2009 High-pressure structural, electronic and optical properties of KMgF$_3$: a first-principles study *J. Alloys Compd.* **484** 597–600

[21] Hiadsi S, Bouafia H, Sahli B, Abidri B, Bouaza A and Akriche A 2016 Structural, mechanical, electronic and thermal properties of KZnF$_3$ and AgZnF$_3$ perovskites: FP-(L) APW+ lo calculations *Solid State Sci.* **58** 1–13

[22] Murtaza G, Sadique G, Aliabad H R, Khalid M N, Naeem S, Afaq A and Ahmad I 2011 First principle study of cubic perovskites: AgTF$_3$ (T = Mg, Zn) *Physica* B **406** 4584–9

[23] Mubarak A A 2018 *Ab initio* study of Ag-based fluoroperovskite AgMF$_3$ (M = Co and Ni) compounds *J. Electron. Mater.* **47** 887–98

[24] Larbi A H, Bouzid F, Hadjab M, Naas A and Hiadsi S 2016 The variation of the gap with hydrostatic pressure of the fluoropervskite RbZnF$_3$ compound *7th African Conf. on Non Destructive Testing (ACNDT)*

[25] Benkabou M H, Harmel M, Haddou A, Yakoubi A, Baki N, Ahmed R and Johan M R 2018 Structural, electronic, optical and thermodynamic investigations of NaXF3 (X = Ca and Sr): First-principles calculations *Chin. J. Phys.* **56** 131–44

[26] Rai D P, Shankar A, Ghimire M P, Khenata R, Omran S B, Syrotyuk S V and Thapa R K 2017 Investigation of the structural, electronic and optical properties of the cubic RbMF$_3$ perovskites (M = Be, Mg, Ca, Sr and Ba) using modified Becke-Johnson exchange potential *Mater. Chem. Phys.* **192** 282–90

[27] Li Z, Wang Y and Liu D X 2017 First-principles study of the correlation between host components and properties of IAIIAF$_3$ cubic perovskite compounds *J. Math. Inf.* **9** 47

[28] Khan S, Zaman S U, Ahmad R, Mehmood N, Arif M and Kim H J 2020 *Ab initio* investigations of structural, elastic, electronic and optical properties of the fluoroperovskite TIXF3 (X = Ca, Cd, Hg, and Mg) compounds *Mater. Res. Express* **6** 125923

[29] Gómez-Peralta J I and Bokhimi X 2021 Ternary halide perovskites for possible optoelectronic applications revealed by artificial intelligence and DFT calculations *Mater. Chem. Phys.* **267** 124710

[30] Perdew J P, Ruzsinszky A, Csonka G I, Vydrov O A, Scuseria G E, Constantin L A and Burke K 2008 Restoring the density-gradient expansion for exchange in solids and surfaces *Phys. Rev. Lett.* **100** 136406

[31] Clark S J, Segall M D, Pickard C J, Hasnip P J, Probert M I, Refson K and Payne M C 2005 First principles methods using CASTEP Z. *Kristallogr. Cryst. Mater.* **220** 567–70

[32] Vanderbilt D 1990 Soft self-consistent pseudopotentials in a generalized eigenvalue formalism *Phys. Rev.* B **41** 7892

[33] Monkhorst H J and Pack J D 1976 Special points for Brillouin-zone integrations *Phys. Rev.* B **13** 5188

[34] Fischer T H and Almlof J 1992 General methods for geometry and wave function optimization *J. Phys. Chem.* **96** 9768–74

[35] Kang J, Lee E C and Chang K J 2003 First-principles study of the structural phase transformation of hafnia under pressure *Phys. Rev.* B **68** 054106

[36] Bouhemadou A 2008 Calculated structural and elastic properties of $M_2InC$ (M = Sc, Ti, V, Zr, Nb, Hf, Ta) *Mod. Phys. Lett.* B **22** 2063–76

[37] Blanco M A, Francisco E and Luana V 2004 GIBBS: isothermal-isobaric thermodynamics of solids from energy curves using a quasi-harmonic Debye model *Comput. Phys. Commun.* **158** 57–72

[38] Birch F 1947 The finite elastic strain of cubic crystals *Phys. Rev. Mater.* **71** 809

[39] Birch F 1978 Finite strain isotherm and velocities for single crystal and polycrystalline NaCl at high pressures and 300 K *J. Geophys. Res.* **83** 1257–68

[40] Vinet P J J R, Ferrante J, Smith J R and Rose J H 1986 A universal equation of state for solids *J. Phys. C: Solid State Phys.* **19** L467

[41] Li C, Lu X, Ding W, Feng L, Gao Y and Guo Z 2008 Formability of $ABX_3$ (X = F, Cl, Br, I) halide perovskites *Acta Crystallogr.* B **64** 702–7

[42] Zhao Y and Zhu K 2016 Organic–inorganic hybrid lead halide perovskites for optoelectronic and electronic applications *Chem. Soc. Rev.* **45** 655–89

[43] Mouna S C, Radjai M, Bouhemadou A, Houatis D, Allali D, Essaoud S S and Bin-Omran S 2023 Structural, elastic, and thermodynamic properties of $BaXCl_3$ (X = Li, Na) perovskites under pressure effect: *ab initio* exploration *Phys. Scr.* **98** 065949

[44] Radjai M, Guechi N and Maouche D 2021 *ab initio* initio study of structural, elastic and electronic properties of hexagonal MAuGe (M = Lu, Sc) compounds (arXiv:2103.15579)

[45] Radjai M, Maouche D, Guechi N, Cheddadi S and Kechidi Z 2019 Investigation of structural and elastic properties of monoclinic $Ba_2P_7X$ (X = Cl, Br, I) Zintl Salts compounds (arXiv:1910.00915)

[46] Dar S A, Srivastava V, Sakalle U K, Rashid A and Pagare G 2018 First-principles investigation on electronic structure, magnetic, mechanical, and thermodynamic properties of $SrPuO_3$ perovskite oxide *Mater. Res. Express* **5** 026106

[47] Radjai M, Bouhemadou A and Bin-Omran S 2022 *ab initio* study of pressure dependence of the structural, elastic, and thermodynamic properties of Al X $Y_3$ (X = B, C) *Phase Transit.* **96** 1–15

[48] Grimvall G 1999 *Thermophysical Properties of Materials* (Elsevier)

[49] Liu Q J, Ran Z, Liu F S and Liu Z T 2015 Phase transitions and mechanical stability of $TiO_2$ polymorphs under high pressure *J. Alloys Compd.* **631** 192–201

[50] Voigt W 1928 *Lehrbuch der Kristallphysik (Textbook of Crystal Physics)* (BG Teubner)

[51] Hill R 1952 The elastic behaviour of a crystalline aggregate *Proc. Phys. Soc.* A **65** 349

[52] Radjai M, Bouhemadou A and Maouche D 2021 Structural, elastic, electronic and optical properties of the half-Heusler ScPtSb and YPtSb compounds under pressure (arXiv:2112.09940)

[53] Karim A M M T, Jubair M, Nuruzzaman M and Zilani M A K 2022 An *ab initio* study on the mechanical stability, spin-dependent electronic properties, molecular orbital predictions, and optical features of antiperovskite $A_3InN$ (A = Co, Ni) *ACS Omega* **7** 13588–603

[54] Khan H, Sohail M, Rahman N, Hussain M, Khan A and Hegazy H H 2022 Theoretical study of different aspects of Al-based fluoroperovskite $AlMF_3$ (M = Cu, Mn) compounds using TB-MBJ potential approximation method for generation of energy *Results Phys.* **42** 105982

[55] Pugh S F 1954 XCII. Relations between the elastic moduli and the plastic properties of polycrystalline pure metals *London, Edinburgh Dublin Phil. Mag. J. Sci.* **45** 823–43

[56] Rahman M A, Mousumi K, Ali M L, Rahman M Z, Hasan S S, Hasan W and Hasan M Z 2023 First-principles calculations to investigate elastic, electronic, optical and thermodynamic properties of $Pt_3X$ (X = Ti, Cu) *Results Phys.* **44** 106141

[57] Anderson O L 1963 A simplified method for calculating the Debye temperature from elastic constants *J. Phys. Chem. Solids* **24** 909–17

[58] Bouhemadou A, Allali D, Bin-Omran S, Al Safi E M A, Khenata R and Al-Douri Y 2015 Elastic and thermodynamic properties of the $SiB_2O_4$ (B = Mg, Zn and Cd) cubic spinels: an *ab initio* FP-LAPW study *Mater. Sci. Semicond. Process.* **38** 192–202

[59] Ranganathan S I and Ostoja-Starzewski M 2008 Universal elastic anisotropy index *Phys. Rev. Lett.* **101** 055504

[60] Ravindran P, Fast L, Korzhavyi P A, Johansson B, Wills J and Eriksson O 1998 Density functional theory for calculation of elastic properties of orthorhombic crystals: application to $TiSi_2$ *J. Appl. Phys.* **84** 4891–904

[61] Luan X, Qin H, Liu F, Dai Z, Yi Y and Li Q 2018 The mechanical properties and elastic anisotropies of cubic $Ni_3Al$ from first principles calculations *Crystals* **8** 307

[62] Gaillac R, Pullumbi P and Coudert F X 2016 ELATE: an open-source online application for analysis and visualization of elastic tensors *J. Condens. Matter Phys.* **28** 275201

[63] Belaroussi T, Benmessabih T, Hamdache F and Amrani B 2008 First-principles study of the structural and thermodynamic properties of $AsNMg_3$ antiperovskite *Physica* B **403** 2649–53

[64] Lu L Y, Cheng Y, Chen X R and Zhu J 2005 Thermodynamic properties of MgO under high pressure from first-principles calculations *Physica* B **370** 236–42

[65] Reshak A H, Khan S, Laref A, Murtaza G and Bila J 2020 Pressure induced physical variations in the lead free fluoropervoskites $XYF_3$ (X = K, Rb, Ag; Y = Zn, Sr, Mg): optical materials *Opt. Mater.* **109** 110325

[66] Korba S A, Meradji H, Ghemid S and Bouhafs B 2009 First principles calculations of structural, electronic and optical properties of $BaLiF_3$ *Comput. Mater. Sci.* **44** 1265–71

[67] Ching-Prado E 2018 Stress dependence of structure, electronic and optical properties of $BaTiO_3$ from WC, VdW-DF-C09 and HSE functional calculations *Ferroelectrics* **535** 171–82

[68] Khan H, Sohail M, Khan R, Raman N, Ullah A, Khan A and Yessoufou K 2022 Theoretical investigations into the different properties of Al-based fluoroperovskite $AlMF_3$ (M = Cr, B) compounds by the TB-MBJ potential method *Materials* **15** 5942

[69] Ahmad M, Rehman G, Ali L, Shafiq M, Iqbal R, Ahmad R and Ahmad I 2017 Structural, electronic and optical properties

of CsPbX$_3$ (X = Cl, Br, I) for energy storage and hybrid solar cell applications *J. Alloys Compd.* **705** 828–39

[70] Laksari S, Chahed A, Abbouni N, Benhelal O and Abbar B 2006 First-principles calculations of the structural, electronic and optical properties of CuGaS$_2$ and AgGaS$_2$ *Comput. Mater. Sci.* **38** 223–30

[71] Sarker S, Rahman M A and Khatun R 2021 Study of structural, elastic, electronics, optical and thermodynamic properties of Hf$_2$PbC under pressure by *ab-initio* method *Comput. Condens. Matter* **26** e00512

[72] Jana D, Sun C L, Chen L C and Chen K H 2013 Effect of chemical doping of boron and nitrogen on the electronic, optical, and electrochemical properties of carbon nanotubes *Prog. Mater. Sci.* **58** 565–635

[73] Yue H, Fang K, Chen T, Jing Q, Guo K, Liu Z and Yao K 2023 First-principle study on correlate structural, electronic and optical properties of Ce-doped BaTiO$_3$ *Crystals* **13** 255

[74] Hussain M I, Khalil R A, Hussain F, Imran M, Rana A M and Kim S 2020 Investigations of structural, electronic, and optical properties of TM-GaO$_3$ (TM = Sc, Ti, Ag) perovskite oxides for optoelectronic applications: a first-principles study *Mater. Res. Express* **7** 015906

[75] Roknuzzaman M, Hadi M A, Abden M J, Nasir M T, Islam A K M A, Ali M S and Naqib S H 2016 Physical properties of predicted Ti$_2$CdN versus existing Ti$_2$CdC MAX phase: an *ab initio* study *Comput. Mater. Sci.* **113** 148–53

[76] Hossain M A, Ali M S and Islam A K M A 2012 Rare earth rhodium borides RRh$_3$B (R = Y, Zr, and Nb): mechanical, thermal and optical properties *Eur. Phys. J.* B **85** 1–7

[77] Miah M K, Hossain K M, Rahman M A, Rasheduzzaman M, Mitro S K, Modak J K and Hasan M Z 2021 Comprehensive study on the physical properties of tetragonal LaTGe$_3$ (T = Rh, Ir, or Pd) compounds: an *ab initio* investigation *AIP Adv.* **11** 025046